

# Magnetic hardness of hexagonal and orthorhombic $\text{Fe}_3\text{C}$ , $\text{Co}_3\text{C}$ , $(\text{Fe-Co})_3\text{C}$ , and their alloys with boron, nitrogen, and transition metals: A first-principles study

Justyn Snarski-Adamski, Mirosław Werwiński,\* and Justyna Rychły-Gruszecka

*Institute of Molecular Physics, Polish Academy of Sciences,*

*M. Smoluchowskiego 17, 60-179 Poznań, Poland*

(Dated: January 30, 2025)

Restrictions on the availability of rare earth metals create a strong demand for new rare-earth-free hard magnetic materials. In this study, we considered a large set of materials that are closely related to orthorhombic  $\text{Fe}_3\text{C}$  (cementite) with the aim of characterizing trends in their intrinsic magnetic properties, highlighting the relation between magnetic properties and the chemical composition, and identifying alloys that are optimal for applications. A comprehensive analysis was conducted on the full concentration ranges of hexagonal ( $\epsilon$ ) and orthorhombic ( $\theta$ ) phases of  $(\text{Fe-Co})_3\text{C}$ ,  $(\text{Fe-Co})_3(\text{B-C})$ ,  $(\text{Fe-Co})_3(\text{C-N})$ , and their alloys with  $3d$ ,  $4d$  and  $5d$  transition metals. The calculations were performed using the density functional theory implemented in the full-potential local-orbital code (FPLO). Calculated properties included formation energies, Curie temperatures, magnetic moments, magnetocrystalline anisotropy energies (MAE), and magnetic hardnesses. The considered compositions exhibit a range of magnetic properties, including soft, semi-hard, and hard magnetic. The materials most promising for hard-magnetic applications are selected Co-rich orthorhombic and hexagonal  $(\text{Fe,Co})_3\text{C}$  alloys. The calculation results do not indicate that substituting with transition metals increases the potential of the alloys for permanent magnet applications. A significant drawback of alloying orthorhombic  $\theta\text{-Fe}_3\text{C}$  (cementite) with transition metals is the notable decline in the Curie temperature. Among the positive outcomes, we found that a considerable proportion of the orthorhombic  $\text{Co}_3(\text{B-C-N})$  alloys are magnetically hard, of which boron substitution raises the Curie temperature and improves stability. By mapping the dependence of MAE on the concentration of elements covering both the  $3d$  (from Fe to Co) and  $2p$  (from B, through C, to N) positions, we have demonstrated for the first time the near isoelectronic nature of MAE. The latter observation may be particularly useful in designing compositions of new magnetically hard materials.

## I. INTRODUCTION

Permanent magnets are an essential component of modern technology [1–3]. Demand for neodymium magnets reached 119.2 thousand tons in 2020 and is growing [4]. However, there are potential risks associated with the use of neodymium magnets, such as limited availability of neodymium and strong fluctuations of its price. The significant increase in price of rare-earth metals that took place around 2011 is referred to as the *2011 rare-earth crisis* [5]. A similar economic situation was repeated in 2022. For the above reasons, it is important to identify new materials for permanent magnet applications that require minimal or no rare earth elements [6–11].

In this work, we will focus on  $\text{Fe}_3\text{C}$ -based alloys intensively studied for more than a decade as promising materials for permanent magnets [12–19].

In this study, we present a first-principles analysis of the hexagonal iron carbide  $\epsilon\text{-Fe}_3\text{C}$  (referred to hereafter as hexa- $\text{Fe}_3\text{C}$ ), the orthorhombic cementite  $\theta\text{-Fe}_3\text{C}$  (referred to hereafter as ortho- $\text{Fe}_3\text{C}$ ), and the corresponding  $\text{Co}_3\text{C}$  phases (hexa- $\text{Co}_3\text{C}$  and ortho- $\text{Co}_3\text{C}$ ). Moreover, we calculate a series of  $\text{Fe}_3\text{C}$  and  $\text{Co}_3\text{C}$  alloys with transition metal elements  $3d$ ,  $4d$ , and  $5d$  and also consider the  $(\text{Fe,Co})_3\text{C}$  and  $(\text{Fe,Co})_3(\text{B,C,N})$  alloys.

When discussing  $\text{Fe}_3\text{C}$  and  $\text{Co}_3\text{C}$  alloys for use as permanent magnets, we will focus primarily on two intrinsic properties of the materials, magnetocrystalline anisotropy energy (MAE) and Curie temperature ( $T_C$ ). The experimental value of the uniaxial magnetocrystalline anisotropy constant of ortho- $\text{Fe}_3\text{C}$  is a moderate  $0.405 \text{ MJ m}^{-3}$  at 5 K [20]. Whereas, the measured Curie temperature for ortho- $\text{Fe}_3\text{C}$  has been measured as 481 K [21] and 483 K [22]. The state of the knowledge on the properties of ortho- $\text{Fe}_3\text{C}$  (cementite) is summarized by Bhadeshia [23]. For ortho- $\text{Co}_3\text{C}$ , the measured Curie temperatures are 498 K [24], 510 K [25], 563 K [26], and 650 K [27]. The results were determined for nanoparticles, and their large dispersion indicates a significant effect of structurization on the magnetic properties of the system. The ortho- $\text{Co}_3\text{C}$  shows an experimental MAE of  $0.74 \pm 0.1 \text{ MJ m}^{-3}$  [27]. Additionally,  $\text{Co}_3\text{C}$  carbide nanocrystals have been confirmed to possess hard magnetic properties [12]. Enhanced magnetocrystalline anisotropy has also been observed in Co-C nanowires, Co-C nanoparticles, and polyphase Fe-Co-C polycrystalline samples [15, 27, 28]. The melt-spun  $\text{Fe}_2\text{CoC}$  alloys show elevated magnetocrystalline anisotropy constant ( $K_1$ ) of  $0.91 \text{ MJ m}^{-3}$  and magnetic moment of  $1.23 \mu_B \text{ atom}^{-1}$  (at 10 K) [17]. In contrast, an exceptionally high  $K_1$  of  $4.6 \text{ MJ m}^{-3}$  has been measured for  $\text{Fe}_2\text{CoC}$  nanoparticles [15].

$\text{Fe}_3\text{C}$  compositions with transition metals were also experimentally studied, among others: Ti, V, Cr, Mn, Ni, and Mo [29–32]. It was determined what effect the selected substitutions have on the lattice parameters [29]

---

\* Corresponding author: Mirosław Werwiński  
Email address: [werwinski@ifmpan.poznan.pl](mailto:werwinski@ifmpan.poznan.pl)

and Curie temperature [30]. It was also found that Cr, Mn, V, and Mo stabilize the alloy, while Ti and Ni destabilize it [31].

Another type of modification of  $\text{Fe}_3\text{C}$  that significantly affects properties is alloying with boron or nitrogen in place of carbon [21, 33]. For example, it has been shown experimentally that going from  $\text{Fe}_3\text{C}$  to  $\text{Fe}_3\text{B}$  the Curie temperature increases linearly from 481 K to 824 K [21].

Recently, based on first-principles calculations combined with a structure prediction algorithm, positive formation energies (indicating instability) have been determined for the well-known iron carbides and for a large set of newly determined iron carbides [47]. Direct studies on  $\text{Fe}_3\text{C}$  were also carried out using first-principle calculations [34, 48]. The average spin magnetic moments have been estimated as 1.50 and 1.40  $\mu_B \text{ atom}^{-1}$  for the hexa- and ortho- $\text{Fe}_3\text{C}$  phases, respectively [48]. For details, like spin magnetic moment on Fe and C sites, please check the Table I.

To improve stability and determine magnetic properties, first-principles calculations have been repeatedly used to model cementite alloys with Cr [36, 38, 44, 49–51], Mn [38, 50], Co [17, 52, 53], and Ni [52, 53]. Whereas, the broader context is complemented by calculations of wide ranges of transition metal substitutions in ortho- $\text{Fe}_3\text{C}$  [37, 54, 55].

First-principles calculations were also made for orthorhombic cementite-type and hexagonal  $\epsilon$  phases of  $\text{Fe}_3\text{B}$  and  $\text{Fe}_3\text{N}$  compounds [34, 56]. The full range of alloy concentrations of ortho- $\text{Fe}_3(\text{C}_{1-y}\text{B}_y)$  was modeled by the supercell method [57]. Furthermore, Al, Si, P, and S were considered at the C site in the cementite [54]. In addition, in our previous work we already considered  $\text{Fe}_{0.7}\text{Co}_{0.3}$  thin films with B, C, and N atoms in interstitial positions [58].

This study, covers the wide ranges of alloying with transition metals, boron, nitrogen, and, going beyond previous reports, focuses on determination of magnetic hardnesses and Curie temperatures – two parameters especially important for permanent magnet applications.

## II. CALCULATIONS DETAILS

The calculations were done using density functional theory (DFT) implemented in the full-potential local-orbital code (FPLO18.00-52) [61]. The FPLO includes relativistic effects in the full four-component formalism [62]. Unless otherwise specified, the generalized gradient approximation (GGA) proposed by Perdew, Burke, and Ernzerhof (PBE) [63] was used. For Brillouin zone integration, a tetrahedron method was used, with a mesh of  $k$ -points set to  $40 \times 40 \times 40$ . All calculations were fully converged with a density criterion of  $10^{-7}$ .

The initial structural data for hexagonal  $\epsilon$ - $\text{Fe}_3\text{C}$  and orthorhombic  $\theta$ - $\text{Fe}_3\text{C}$  phase were taken from experiment [59, 60], see Table II and Fig. 1. Hexa- and ortho- $\text{Co}_3\text{C}$  structures were prepared using initial data for  $\text{Fe}_3\text{C}$  phases. The volumes of all considered structures were

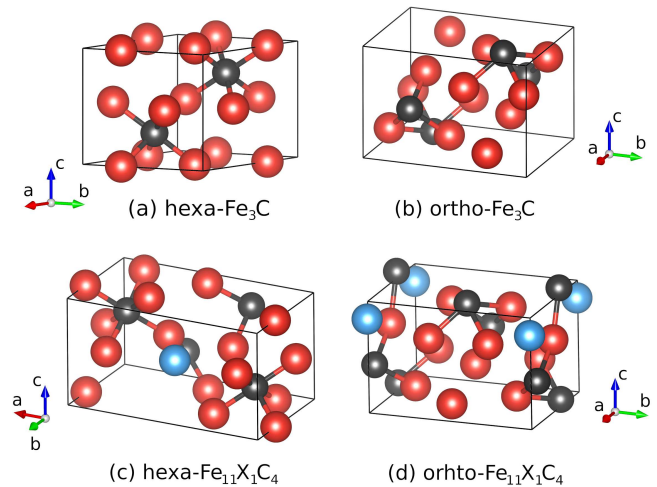


FIG. 1. Crystal structures of (a) hexa- $\text{Fe}_3\text{C}$  and (b) ortho- $\text{Fe}_3\text{C}$ , together with corresponding structures of (c,d) hexa- and ortho- $\text{Fe}_{11}\text{X}_1\text{C}_4$  alloys substituted with transition metal element X. Iron, carbon, and transition metal atoms are represented by red, black, and blue spheres, respectively.

optimized. For hexagonal structures, the ratio of  $c/a$  lattice parameters was optimized as well. Wyckoff’s positions were optimized in each system using forces with convergence criterion set to  $10^{-3} \text{ eV \AA}^{-1}$  within a scalar-relativistic approach and with spin polarization, see Table II. The crystal structures were visualized with the VESTA program [64].

To determine the magnetocrystalline anisotropy energy (MAE), following the completion of self-consistent scalar-relativistic calculations, single iterations of fully relativistic calculations were conducted for orthogonal directions of the magnetization. To analyze the effect of the form of the exchange-correlation potential on the magnetic moment and MAE, the von Barth and Hedin (vBH) [65], Perdew and Zunger (PZ) [66], Perdew and Wang (PW92) [67], and exchange-only (x-only) forms of the local spin density approximation (LSDA) were used in addition to the Perdew-Burke-Ernzerhof (PBE) [63] potential used throughout the paper. In order to ascertain the dependency of the MAE on the magnetic moment, a fully relativistic approach was employed, utilizing of the fixed-spin-moment (FSM) method.

The virtual crystal approximation (VCA) was used to model the  $(\text{Fe,Co})_3\text{C}$  alloys and alloying with B and N at the C position. For the pseudobinary  $(\text{Fe,Co})_3(\text{B,C,N})$  alloys, a total of 231 compositions for both hexagonal and orthorhombic phase was prepared and evaluated. In order to calculate structures with different percentages of Fe and Co, the lattice parameters and Wyckoff positions were averaged proportionally according to the Fe and Co content of the structure.

To consider  $\frac{1}{12}$  substitution of the Fe atoms with  $3d$ ,  $4d$ , and  $5d$  elements, the symmetry of both unit cells was reduced, see Fig. 1. In the case of hexa- $\text{Fe}_{11}\text{X}_1\text{C}_4$  alloys, the space group was reduced to  $P121$ , while for ortho-

TABLE I. Total spin magnetic moments [total  $m_s$  ( $\mu_B$  f.u.<sup>-1</sup>)] calculated for hexa-Fe<sub>3</sub>C, hexa-Co<sub>3</sub>C, ortho-Fe<sub>3</sub>C and ortho-Co<sub>3</sub>C, together with contributions from Fe, Co, and C sites [ $m_s(\text{Fe/Co/C})$  ( $\mu_B$  atom<sup>-1</sup>)]. For orthorhombic phases, magnetic moments on general and special positions of Fe and Co are presented. Our results obtained using the FPLO18 code with PBE exchange-correlation potential are compared with previous calculation outcomes from literature.

hexa-Fe <sub>3</sub> C				
	$m_s(\text{Fe})$	$m_s(\text{C})$	total $m_s$	
FPLO, GGA(PBE) [this work]	2.12	-0.30	6.04	
VASP, PAW, GGA [17]	-	-	5.92	
CASTEP, PBE-GGA [34, 35]	(2.04 - 2.23)	(-0.26 - -0.24)	(5.90 - 6.42)	
hexa-Co <sub>3</sub> C				
	$m_s(\text{Co})$	$m_s(\text{C})$	total $m_s$	
FPLO, GGA(PBE) [this work]	1.03	-0.12	2.95	
VASP, PAW, GGA [17]	-	-	2.76	
ortho-Fe <sub>3</sub> C				
	$m_s(\text{Fe}^g)$	$m_s(\text{Fe}^s)$	$m_s(\text{C})$	total $m_s$
FPLO, GGA(PBE) [this work]	1.93	2.01	-0.28	5.56
VASP, PAW, GGA [17, 36-41]	(1.84 - 1.93)	(1.92 - 1.98)	(-0.12 - -0.14)	(5.52 - 5.72)
VASP, PW91, USPP-GGA [42]	1.95	1.99	-0.16	5.73
WIEN2K, FP-LAPW, GGA [43]	1.96	1.97	-0.13	5.76
QUANTUM ESPRESSO, PWscf, GGA [44]	2.04	2.09	-0.24	5.90
CASTEP, GGA [35, 45, 46]	(1.83 - 1.90)	(1.94 - 1.98)	(-0.24 - -0.23)	(5.55 - 5.56)
ortho-Co <sub>3</sub> C				
	$m_s(\text{Co}^g)$	$m_s(\text{Co}^s)$	$m_s(\text{C})$	total $m_s$
FPLO, GGA(PBE) [this work]	1.12	1.02	-0.11	3.16
VASP, PAW, GGA [17, 41]	0.98	1.07	-0.05	(2.98 - 3.12)

TABLE II. The initial and optimized lattice parameters and Wyckoff positions for hexa-Fe<sub>3</sub>C (s.g.  $P6_322$ ) and ortho-Fe<sub>3</sub>C (s.g.  $Pnma$ ) phases. The geometry optimization was performed with the FPLO18 code using the PBE potential.

Initial structural data				
Phase	Space group	Lattice parameters	Wyckoff positions	
hexa-Fe <sub>3</sub> C [59]	$P6_322$ (182)	$a = b = 4.767$	Fe = 0.333	0 0
		$c = 4.354$	C =	1/3 2/3 3/4
		$a = 5.092$	Fe <sup>g</sup> = 0.1834	0.0689 0.3344
ortho-Fe <sub>3</sub> C [60]	$Pnma$ (62)	$b = 6.741$	Fe <sup>s</sup> = 0.0388	0.25 0.8422
		$c = 4.527$	C =	0.8764 0.25 0.4426
Optimized structural data				
Phase	Space group	Lattice parameters	Wyckoff positions	
hexa-Fe <sub>3</sub> C	$P6_322$ (182)	$a = b = 4.677$	Fe = 0.3196	0 0
		$c = 4.344$	C =	1/3 2/3 3/4
hexa-Co <sub>3</sub> C	$P6_322$ (182)	$a = b = 4.5497$	Co = 0.32348	0 0
		$c = 4.4095$	C =	1/3 2/3 3/4
ortho-Fe <sub>3</sub> C	$Pnma$ (62)	$a = 5.0510$	Fe <sup>g</sup> = 0.1765	0.0664 0.3322
		$b = 6.6867$	Fe <sup>s</sup> = 0.0337	0.25 0.8392
		$c = 4.4906$	C =	0.8762 0.25 0.4381
ortho-Co <sub>3</sub> C	$Pnma$ (62)	$a = 4.996$	Co <sup>g</sup> = 0.1805	0.0683 0.3314
		$b = 6.614$	Co <sup>s</sup> = 0.0372	0.25 0.8451
		$c = 4.442$	C =	0.8794 0.25 0.4479

(Fe/Co)<sub>11</sub>X<sub>1</sub>C<sub>4</sub> alloys, the space group was reduced to  $P1m1$ . For supercells, the mesh of  $k$ -points was set to  $25 \times 25 \times 25$ , while the charge density criterion was  $10^{-7}$ . In all supercells, the lattice parameters were taken as they were in the initial optimized compounds, whereas the Wyckoff positions were optimized using forces. The choice of a substitution concentration of  $\frac{1}{12}$  is based on

the trade-off between the relatively low concentration value and the computation time. Within the supercell method, an alternative concentration of  $\frac{1}{24}$  would have to be based on twice the elemental cell, which would increase calculation time by several times.

Formation energies ( $E_f$ ) of Fe<sub>11</sub>X<sub>1</sub>C<sub>4</sub> alloys were cal-

culated from equation:

$$E_f = E_{Fe_{11}X_1C_4} - 11E_{Fe} - E_X - 4E_C, \quad (1)$$

where  $E_{Fe_{11}X_1C_4}$ ,  $E_{Fe}$ ,  $E_C$ , and  $E_X$  are the total energies of the  $Fe_{11}X_1C_4$  supercell and the crystals of iron, carbon (graphite), and transition metal (X), respectively. To determine the total energies, we prepared and optimized the geometry of  $3d$ ,  $4d$ , and  $5d$  crystals. The formation energies of hexa- $Co_{11}X_1C_4$  compositions were calculated analogically. The formation energies are determined for the ground state, that is, at 0 K.

For the hexagonal crystal system, the MAE can be estimated from the difference in energies calculated for magnetization along the unique crystal axis and the axis perpendicular to it. It can give both non-negative and negative values, for perpendicular and in-plane magnetocrystalline anisotropy, respectively.

Following our approach for calculating the MAE in orthorhombic structures [68], we have applied the same method in this work. The axis of easy magnetization is defined by the lowest energy of the three fully relativistic quantization directions along the main crystal axes ([100], [010], and [001] along  $a$ ,  $b$ , and  $c$ , respectively). For each composition, we define an axis with the lowest energy ( $E_1$ ), medium energy ( $E_2$ ), and highest energy ( $E_3$ ). The MAE of an orthorhombic system is determined by the difference between the medium and lowest energy, which gives us only non-negative MAE values. To complete the determination of MAE in the orthorhombic structure, we introduced the  $DE_{32}$  parameter describing the anisotropy energy between  $E_3$  and  $E_2$ . For the experimental determination of the effective MAE, similar approach was used by Zhdanova *et al.* [69].

Another key parameter when discussing permanent magnet applications is magnetic hardness [11], which can be expressed as :

$$\kappa = \sqrt{\frac{K}{\mu_0 M_s^2}}, \quad (2)$$

where  $K$  is magnetocrystalline anisotropy constant (interpreted as MAE),  $\mu_0$  is vacuum permeability, and  $M_s$  is saturation magnetization. The latter might be given as:

$$M_s = \frac{m_s + m_l}{V}, \quad (3)$$

where  $m_s$  is total spin magnetic moment,  $m_l$  is total orbital magnetic moment, and  $V$  is unit cell volume. While  $\kappa > 1$  denotes hard magnetic materials, it is assumed that  $0.1 < \kappa < 1$  defines the range of semi-hard magnetic materials [11]. To use the semi-hard materials as permanent magnets, the condition that  $\kappa \gtrsim 0.5$  should be met [11].

Curie temperature ( $T_C^{\text{MFT}}$ ) of  $(Fe_{0.916}X_{0.084})_3C$  alloys with the  $3d$ ,  $4d$ , and  $5d$  transition metals (X) were calculated using mean-field theory [70, 71]. Here, mean-field theory is an approximation for fluctuations in configuration of magnetic moment orientations, where all interactions with any body are replaced by an averaged

interaction [70]. When calculating the mean-field Curie temperature ( $T_C^{\text{MFT}}$ ), a coherent potential approximation (CPA) procedure can be used to average and iterate to self-consistency [70, 72]. The  $(Fe_{0.916}X_{0.084})_3C$  concentration, modeled here with CPA, was chosen to match the  $Fe_{11}X_1C_4$  concentration, modeled with supercell method. We used the:

$$k_B T_C^{\text{MFT}} = \frac{2}{3} \frac{E_{\text{DLM}} - E_{\text{FM}}}{c}, \quad (4)$$

equation. Here,  $E_{\text{DLM}}$  and  $E_{\text{FM}}$  are the total energies of the paramagnetic and ferromagnetic solutions,  $k_B$  is Boltzmann's constant, and  $c$  is the number of *magnetic* atoms in formula. For  $Fe_3C$  we assume  $c$  equal 3. To model the paramagnetic configuration, we used the disordered local moment (DLM) approach [73] with the coherent potential approximation (CPA) [72]. In the DLM approach, the local magnetic moments can rotate, and the self-consistent calculations are conducted for the given arrangement of them. Numerous magnetic moment orientations are calculated and averaged. The paramagnetic state is determined by taking the total magnetic moment equal to zero. A ferromagnetic (FM) ground state, on the other hand, is defined as an equilibrium configuration of parallel collinear magnetic moments. Scalar-relativistic DLM-CPA calculations were conducted using the FPLO5 code, which is the most recent version of the FPLO code that incorporates CPA. However, the FPLO5 code lacks the PBE-GGA implementation, forcing the use of the LDA-PW92 exchange-correlation potential for CPA calculations [67].

### III. RESULTS AND DISCUSSION

This paper consists of four parts. In the first, we discuss  $Fe_3C$  and  $Co_3C$  compounds. In the second, the  $(Fe,Co)_3C$  alloys. In the third, transition metal substitutions in  $Fe_3C$  and  $Co_3C$  compounds. In the fourth, B and N substitutions at the C position in  $(Fe,Co)_3C$  alloys. Each time, we consider both hexagonal and orthorhombic phases.

#### III.1. $Fe_3C$ and $Co_3C$ compounds

In this section, dedicated to the  $Fe_3C$  and  $Co_3C$  compounds, we will present their densities of states, examine how the choice of the exchange-correlation potential affects the obtained values of magnetic moments and magnetocrystalline anisotropy energy (MAE), and study the dependence of MAE on the magnetic moment. We started this study from the geometry optimization of considered phases, and the optimized structural parameters are presented in Table II.

The experimental standard enthalpy of formation ( $\Delta H_f^0$ ) for  $Fe_3C$  is  $4.7 \pm 1.1$  kJ mol<sup>-1</sup> ( $0.049 \pm 0.011$  eV atom<sup>-1</sup>) and for  $Co_3C$  is  $2.4 \pm 1.1$  kJ mol<sup>-1</sup>



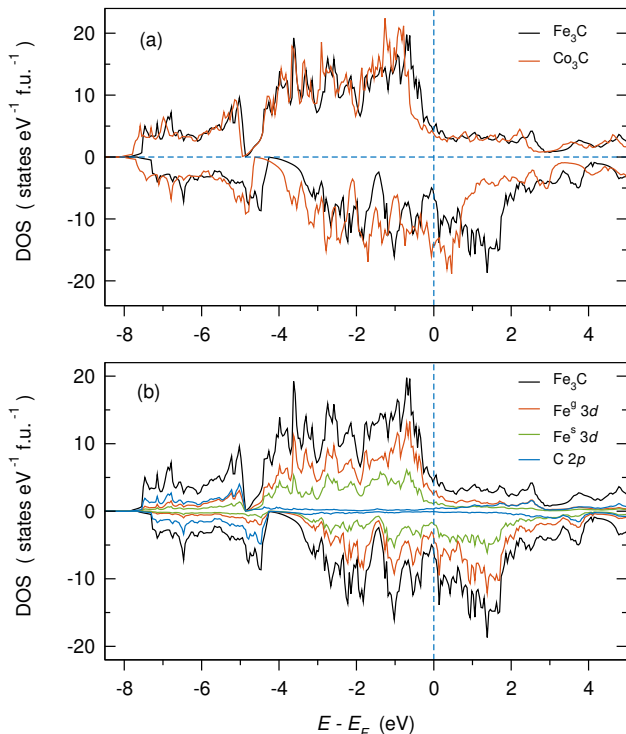


FIG. 2. Densities of states (DOS) for ortho-Fe<sub>3</sub>C and ortho-Co<sub>3</sub>C. The calculations were performed with the FPLO18 code using the PBE exchange-correlation potential.

( $0.025 \pm 0.011$  eV atom<sup>-1</sup>) [74]. Positive enthalpy values indicate instability. Similarly, the previously calculated corresponding formation energies are positive and are 0.016 eV atom<sup>-1</sup> [54] and 0.07 eV atom<sup>-1</sup> [49] for ortho-Fe<sub>3</sub>C and 0.05 eV atom<sup>-1</sup> for ortho-Co<sub>3</sub>C [19]. The formation energies calculated in this work are positive for all four compounds considered in this section and equal to 0.085 eV atom<sup>-1</sup> for hexa-Fe<sub>3</sub>C, 0.70 eV atom<sup>-1</sup> for hexa-Co<sub>3</sub>C, 0.055 eV atom<sup>-1</sup> for ortho-Fe<sub>3</sub>C, and 0.14 eV atom<sup>-1</sup> for ortho-Co<sub>3</sub>C. Orthorhombic phases have lower energies than hexagonal ones, suggesting that Fe<sub>3</sub>C and Co<sub>3</sub>C will prefer the cementite-type structure. The formation energies are also relatively low, giving the possibility of stabilizing the compounds with additional factors such as alloying or the presence of a second phase. Nanoparticles of ortho-Co<sub>3</sub>C were successfully synthesized [13, 75] and the bulk form of ortho-Co<sub>3</sub>C has been obtained under high pressure (above 4.8 GPa) [19]. Another method of stabilizing ortho-Co<sub>3</sub>C is its alloying with a stable isostructural Co<sub>3</sub>B phase [76].

For the application of the material in permanent magnets, it is important that its Curie temperature far exceeds the room temperature. For metastable hexa-Fe<sub>3</sub>C, the Curie temperature is difficult to determine and only an approximate experimental value of  $T_C \geq 653$  K is given [77]. Whereas, off-stoichiometric hexa-Fe<sub>2.2</sub>C has  $T_C$  of about 723 K [78]. The calculated  $T_C$  for hexa-Fe<sub>3</sub>C is 1040 K, which is much higher than the mentioned experimental estimation ( $T_C \geq 653$  K). The observed difference in  $T_C$  may come from both the known

TABLE III. Calculated magnetic properties of hexagonal and orthorhombic (Fe<sub>1-x</sub>Co<sub>x</sub>)<sub>3</sub>C alloys. Spin and orbital magnetic moments [ $m_s$  and  $m_l$  ( $\mu_B$  per atom or f.u.)], magnetocrystalline anisotropy energy [MAE (MJ m<sup>-3</sup>)], and magnetic hardness [ $\kappa$ ]. Magnetic moments on transition-metal (TM) elements for ortho-(Fe<sub>1-x</sub>Co<sub>x</sub>)<sub>3</sub>C alloys are given for both general and special non-equivalent crystallographic sites. The increase in Co concentration  $x$  is expressed as an increase in the atomic number of the transition metal (TM) element; from 26.0 for Fe to 27.0 for Co. The calculations were performed with the FPLO18 code using the PBE potential and virtual crystal approximation.

Hexagonal	Atomic number of TM				
	26.0	26.2	26.7	26.9	27.0
$m_s(\text{Fe/Co})$	2.12	1.97	1.44	1.17	1.03
$m_s(\text{C})$	-0.30	-0.27	-0.18	-0.14	-0.12
total $m_s$	6.04	5.65	4.14	3.38	2.95
$m_l(\text{Fe/Co})$	0.053	0.052	0.049	0.046	0.040
$m_l(\text{C})$	0.00	0.00	0.00	0.00	0.00
total $m_l$	0.16	0.16	0.15	0.14	0.12
MAE	0.68	1.07	-1.46	0.75	-0.15
$\kappa$	0.63	0.83	0.00	1.13	0.00
Orthorhombic	Atomic number of TM				
	26.0	26.1	26.6	26.9	27.0
$m_s(\text{Fe}^g/\text{Co}^g)$	1.93	1.90	1.52	1.24	1.12
$m_s(\text{Fe}^s/\text{Co}^s)$	2.01	1.99	1.47	1.14	1.02
$m_s(\text{C})$	-0.28	-0.26	-0.18	-0.12	-0.11
total $m_s$	5.56	5.53	4.34	3.51	3.16
$m_l(\text{Fe}^g/\text{Co}^g)$	0.042	0.044	0.038	0.035	0.034
$m_l(\text{Fe}^s/\text{Co}^s)$	0.054	0.055	0.050	0.048	0.043
$m_l(\text{C})$	0.00	0.00	0.00	0.00	0.00
total $m_l$	0.14	0.14	0.14	0.12	0.12
MAE	0.11	0.37	0.73	0.82	0.67
$\kappa$	0.21	0.40	0.70	0.91	0.91

overestimation of  $T_C$  in the mean-field theory and the underestimation of the experimental value. Because, as our calculations indicate, the hexa-Co<sub>3</sub>C phase has a much higher formation energy than the other phases under consideration, it is much more difficult to stabilize, and we have not found literature experimental results on both its synthesis and Curie temperature. The  $T_C$  value we determined for hexa-Co<sub>3</sub>C is 310 K.

The experimental Curie temperatures of ortho-Fe<sub>3</sub>C is equal to about 481 K [21] or 483 K [22], while our calculations indicate 570 K, overestimating the experimental value by about 20%, which is the typical behavior of the mean-field  $T_C$  results [79–81]. The experimental Curie temperature for ortho-Co<sub>3</sub>C can be estimated from the results for ortho-Co<sub>3</sub>C-based nanoparticles, but these are ambiguous and depend on the specific properties of the nanoparticles. For ortho-Co<sub>3</sub>C-based nanoparticles, we encounter the following Curie temperatures: 498 K [24], 510 K [25], 563 K [26], and 650 K [27].  $T_C$  calculated by us for ortho-Co<sub>3</sub>C is equal to 458 K. The observed discrepancy between the mean-field result and measure-

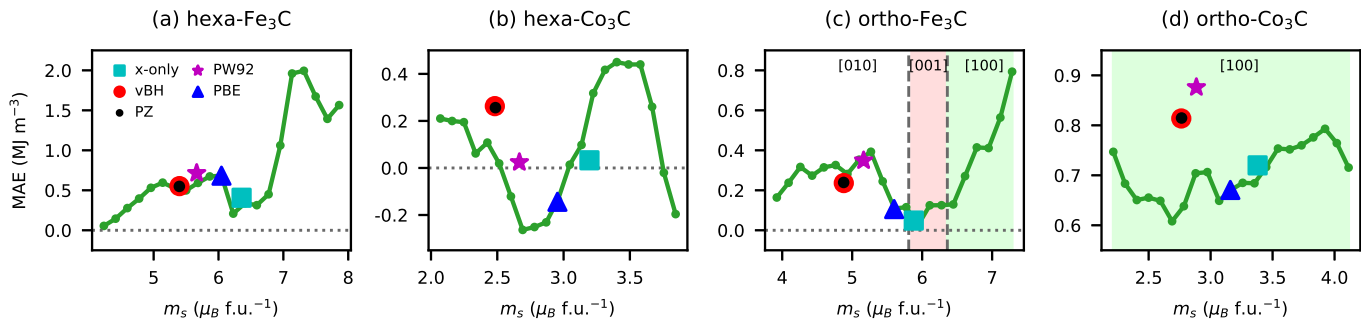


FIG. 3. The dependence of the magnetocrystalline anisotropy energy (MAE) on the spin magnetic moment ( $m_s$ ) for (a) hexa- $\text{Fe}_3\text{C}$ , (b) hexa- $\text{Co}_3\text{C}$ , (c) ortho- $\text{Fe}_3\text{C}$ , and (d) ortho- $\text{Co}_3\text{C}$ . The calculations were performed with the FPLO18 code using the Perdew-Burke-Ernzerhof (PBE) exchange-correlation potential. Equilibrium values of MAE and  $m_s$  were obtained using functionals of von Barth and Hedin (vBH), Perdew and Zunger (PZ), Perdew and Wang 92 (PW92), and LDA exchange-only (x-only), besides Perdew-Burke-Ernzerhof (PBE) in the generalized gradient approximation (GGA). They are represented by symbols. The structures with different axes of easy magnetization are distinguished by different background colors: white for [010], light red for [001], and light green for [100]. In the case of ortho- $\text{Co}_3\text{C}$  there is one easy axis for the whole considered range of magnetic moments, namely [100].

TABLE IV. Total spin magnetic moments [ $m_s$  ( $\mu_B$  f.u. $^{-1}$ )] and the magnetocrystalline anisotropy energies [MAE ( $\text{MJ m}^{-3}$ )] calculated for hexa- $\text{Fe}_3\text{C}$ , hexa- $\text{Co}_3\text{C}$ , ortho- $\text{Fe}_3\text{C}$ , and ortho- $\text{Co}_3\text{C}$ . The equilibrium values were obtained using the von Barth and Hedin (vBH), Perdew and Zunger (PZ), Perdew and Wang 92 (PW92), Perdew-Burke-Ernzerhof (PBE), and LDA exchange-only (x-only) exchange-correlation potentials ( $V_{xc}$ ). The calculations were performed with the FPLO code. At the first line, the VASP-PAW-PBE results from Ref. [17] are presented.

$V_{xc}$	hexa- $\text{Fe}_3\text{C}$		hexa- $\text{Co}_3\text{C}$		ortho- $\text{Fe}_3\text{C}$		ortho- $\text{Co}_3\text{C}$	
	$m_s$	MAE	$m_s$	MAE	$m_s$	MAE	$m_s$	MAE
PBE [17]	5.92	0.57	2.76	0.02	5.52	0.05	3.12	0.81
PBE	6.05	0.68	2.95	-0.15	5.56	0.11	3.16	0.67
vBH	5.40	0.55	2.48	0.26	4.88	0.24	2.76	0.81
PZ	5.40	0.55	2.48	0.26	4.88	0.24	2.77	0.81
PW92	5.66	0.71	2.67	0.02	5.16	0.35	2.89	0.88
x-only	6.36	0.41	3.20	0.03	5.88	0.05	3.38	0.72

ments confirms the significant effect of nanostructuring on the magnetic properties of ortho- $\text{Co}_3\text{C}$  nanoparticles.

Figure 2 presents the densities of states (DOS) calculated for orthorhombic  $\text{Fe}_3\text{C}$  and  $\text{Co}_3\text{C}$ . The valence band of ortho- $\text{Fe}_3\text{C}$  is dominated by Fe  $3d$  and C  $2p$  orbitals, between which a clear hybridization is visible. The spin polarization of the valence band is noticeably stronger for  $\text{Fe}_3\text{C}$ . For densities of states for hexagonal phases, see *Supplementary Material*.

The total spin magnetic moments, corresponding to the spin polarization in the DOS, are 5.56 and 3.16  $\mu_B$  f.u. $^{-1}$  for ortho- $\text{Fe}_3\text{C}$  and ortho- $\text{Co}_3\text{C}$ , respectively. The values of calculated total and partial spin magnetic moments are summarized in the Table III. In the Table I, we have further compared our results (obtained with the full-potential PBE approach) with those from the literature. Given the differences in the calcu-

lation methods used, we rate the level of agreement as good. Later, we will discuss how the choice of exchange-correlation potential affects the spin magnetic moment.

The spin magnetic moment on the Fe atom, determined in our PBE calculations, shows a higher value for hexa- $\text{Fe}_3\text{C}$  (2.12  $\mu_B$ ) and lower values for ortho- $\text{Fe}_3\text{C}$  (1.93 and 2.01  $\mu_B$  for general and special Fe positions, respectively). All values are smaller than the magnetic moments for bcc Fe (2.17  $\mu_B$  [82] or 2.20  $\mu_B$  [83]). In contrast, the hexa- $\text{Co}_3\text{C}$  phase exhibits smaller spin magnetic moments on Co atoms (1.02  $\mu_B$ ) than the ortho- $\text{Co}_3\text{C}$  phase (1.02 and 1.12  $\mu_B$  for special and general Co positions, respectively). The  $m_s$  values for bulk fcc Co are higher (1.66  $\mu_B$  [82]; 1.58  $\mu_B$  [84]) than those calculated for  $\text{Co}_3\text{C}$ .

In the present work, our aim is not to repeat the calculation of magnetic moments, which, as we see in the Table I, has already been done, but to calculate the magnetocrystalline anisotropy energies (MAE) and determine magnetic hardness of considered materials. The MAE values calculated with PBE functional (at 0 K) are 0.68, -0.14, 0.11, and 0.67  $\text{MJ m}^{-3}$  for hexa- $\text{Fe}_3\text{C}$ , hexa- $\text{Co}_3\text{C}$ , ortho- $\text{Fe}_3\text{C}$  and ortho- $\text{Co}_3\text{C}$ , respectively, see Table IV. The calculated MAE of ortho- $\text{Co}_3\text{C}$  is in agreement with experimental magnetocrystalline anisotropy constant determined for ortho- $\text{Co}_3\text{C}$  nanoparticles as  $0.74 \pm 0.1$   $\text{MJ m}^{-3}$  [27]. The corresponding MAE values calculated within projector augmented wave PBE method are 0.57, 0.02, 0.05, and 0.81  $\text{MJ m}^{-3}$  for hexa- $\text{Fe}_3\text{C}$ , hexa- $\text{Co}_3\text{C}$ , ortho- $\text{Fe}_3\text{C}$  and ortho- $\text{Co}_3\text{C}$ , respectively [17], please check Table IV. The similarity between two sets of computational results is qualitatively good, whereas the quantitative differences come most probably from the shape approximation of the potential used by Wu *et al.* [17]. Another theoretical approach determines MAE of ortho- $\text{Co}_3\text{C}$  as between 0.8 and 0.9  $\text{MJ m}^{-3}$  [27], identifying ortho- $\text{Co}_3\text{C}$  phase as hard magnetic. Since all the mentioned results are calculated for a temperature of 0 K and additionally depend on the approximation used,

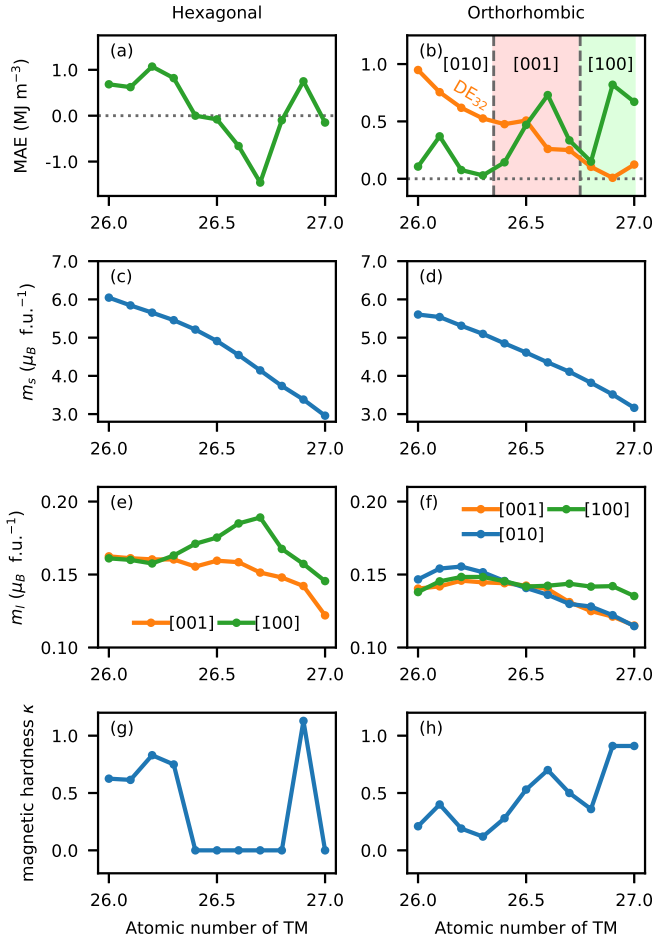


FIG. 4. Intrinsic properties calculated for hexa- and ortho- $(\text{Fe}_{1-x}\text{Co}_x)_3\text{C}$  alloys. The increase in Co concentration  $x$  is expressed as an increase in the atomic number of the transition metal (TM) element; from 26 (Fe) to 27 (Co). (a, b) The magnetocrystalline anisotropy energy (MAE) is represented by the green line with markers, and the energy difference between the two higher energies of three energies calculated for three orthogonal magnetization directions ( $\text{DE}_{32} = E_3 - E_2$ ) by the orange line with markers. (c-f) The total spin ( $m_s$ ) and orbital ( $m_l$ ) magnetic moments, and (g, h) the magnetic hardness ( $\kappa$ ). The concentration range for panel (b) is divided into regions characterized by the magnetic easy axes. Calculations were performed with the virtual crystal approximation (VCA) using the FPLO18 code with PBE exchange-correlation potential.

they should be interpreted with due caution. In order to establish a context for the PBE-MAE results, we will present an analysis of the impact of the form of exchange-correlation potential on the MAE values and the relation between values of MAE and spin magnetic moment.

In our previous works, we demonstrated that the calculated MAE values for  $\text{CeFe}_{12}$  and  $\text{MnB}$  depend on the choice of the exchange-correlation potential [68, 85]. We also showed there, that the MAE is correlated with the spin magnetic moment ( $m_s$ ). Here, we performed MAE and  $m_s$  calculations for the  $\text{Fe}_3\text{C}$  and  $\text{Co}_3\text{C}$  compounds using five forms of exchange-correlation poten-

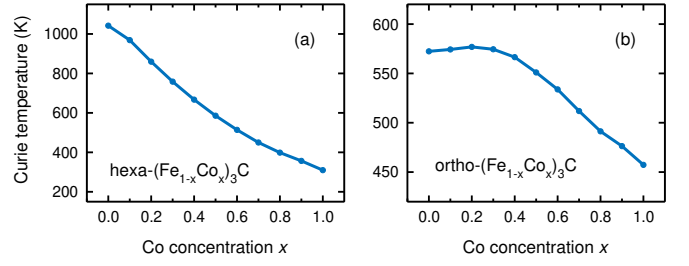


FIG. 5. The mean-field-theory Curie temperatures ( $T_C^{\text{MFT}}$ ) calculated for (a) hexa- and (b) ortho- $(\text{Fe}_{1-x}\text{Co}_x)_3\text{C}$  alloys as a function of Co concentration. The results were obtained using the FPLO5 code and the Perdew and Wang (PW92) functional. The chemical disorder was modeled with coherent potential approximation (CPA). The paramagnetic state was modeled using the disorder local moment (DLM-CPA) method.

tial: Perdew-Burke-Ernzerhof (PBE), von Barth and Hedin (vBH), Perdew and Zunger (PZ), Perdew and Wang 92 (PW92), and LSDA exchange only ( $x$ -only). The self-consistent equilibrium results of MAE and  $m_s$  are shown in Fig. 3, and in Table IV. For each phase, the calculated magnetic moment increases going from vBH and PZ, through PW92, PBE, to the  $x$ -only potential. In the case of MAE, there is a scattering of results with a range of up to about  $0.4 \text{ MJ m}^{-3}$ . However, we do not observe any clear trends in the MAE values. In contrast, the magnetic moments increase in each case with the following order of exchange-correlation potentials: vBH/PZ  $\rightarrow$  PW92  $\rightarrow$  PBE  $\rightarrow$   $x$ -only. In the case of referred ortho- $\text{Co}_3\text{C}$ , alternative functionals result in MAE values that are even higher than those obtained with PBE. Thus, ortho- $\text{Co}_3\text{C}$  appears to be a promising hard-magnetic material, regardless of the approximation used.

Furthermore, we performed calculations of the dependencies of MAE on the fixed spin magnetic moment (FSM), see Fig. 3. We observe, that the dependencies of MAE on fixed spin magnetic moment overlap with equilibrium data points calculated with different functionals.

For hexa- $\text{Fe}_3\text{C}$ , in the whole range of magnetic moments, we observe positive MAE values, implying uniaxial magnetocrystalline anisotropy. The MAE ranges from about 0 to  $2 \text{ MJ m}^{-3}$ . Unfortunately, while lowering the magnetic moment of the system is a relatively straightforward task, engineering an increase in the magnetic moment of  $\text{Fe}_3\text{C}$  can be difficult. It is because  $\text{Fe}_3\text{C}$  has one of the highest magnetic moments among isostructural compounds, and Fe substitution by both Mn and Co leads to a lower magnetic moment.

The magnetic moment of  $\text{Co}_3\text{C}$  phases is about half that of  $\text{Fe}_3\text{C}$  phases. For hexa- $\text{Co}_3\text{C}$ , with increasing magnetic moment, we observe both positive and negative values of MAE, which indicate changes between easy-axis and easy-plane types of magnetocrystalline anisotropy, respectively. All MAE values determined for hexa- $\text{Co}_3\text{C}$  phase classify it as a magnetically soft material.

In the case of ortho- $\text{Fe}_3\text{C}$  we observe somewhat lower

equilibrium magnetic moments than for hexa-Fe<sub>3</sub>C. For ortho-Fe<sub>3</sub>C, with increasing magnetic moment, the axis of easy magnetization undergoes a change from [010] to [001] and subsequently to [100]. The calculated equilibrium MAE values range from 0.05 to 0.35 MJ m<sup>-3</sup>. For the highest considered magnetic moments, above 7 μ<sub>B</sub> f.u.<sup>-1</sup>, the MAE increases up to 0.8 MJ m<sup>-3</sup>. Unfortunately, as we have already said for hexa-Fe<sub>3</sub>C counterpart, raising the magnetic moment of ortho-Fe<sub>3</sub>C might be a difficult task. While previous experiments on Fe<sub>3</sub>(B,C) borocarbides have demonstrated that substituting C by B can result in an approximate 10% increase in the magnetic moment of the system [21], this would still not be sufficient to reach the high MAE range.

In the ortho-Co<sub>3</sub>C system, the obtained PBE-MAE values vary only slightly with the change of the spin magnetic moment, from 0.6 to 0.8 MJ m<sup>-3</sup>. The equilibrium MAE values calculated in LDA (vBH, PZ, and PW92) exceed this range and reach 0.9 MJ m<sup>-3</sup>. As we said already in the previous section, the calculated MAE of ortho-Co<sub>3</sub>C is in agreement with experimental magnetocrystalline anisotropy constant determined for ortho-Co<sub>3</sub>C nanoparticles as 0.74±0.1 MJ m<sup>-3</sup> [27]. Since the observed MAE values are relatively high and the magnetic moments are low, the magnetic hardness is close or above one for the whole considered range of fixed spin magnetic moments.

In summary, from the perspective of magnetic hardness, the ortho-Co<sub>3</sub>C phase deserves the most attention. Calculations suggest that magnetic hardness close to unity should persist not only at 0 K, but also at room temperature when the magnetic moment decreases. In addition, previous experiments show high values of the magnetic anisotropy constant for ortho-Co<sub>3</sub>C nanoparticles and Curie temperatures above 500 K. However, the relatively high price of cobalt works against the potential applications of this system. Having determined the magnetic hardness of Fe<sub>3</sub>C and Co<sub>3</sub>C compounds, in the next section we will address the full ranges of intermediate concentrations of (Fe,Co)<sub>3</sub>C alloys.

### III.2. (Fe,Co)<sub>3</sub>C alloys

Since Fe and Co have consecutive atomic numbers of 26 and 27, their alloys can be modeled using a virtual atom with a fractional atomic number determined by the concentration of the elements. Our goal is to study how the MAE of the system changes with Co concentration and identify promising compositions with elevated MAE. In our attempt we are motivated by previous studies, such as for FeCo, (Fe,Co)<sub>2</sub>B and (Fe,Co)<sub>16</sub>C alloys [86–88], which showed higher MAE values for intermediate compositions than for compounds at the extremes of the Fe/Co range. Moreover, we will determine how the Curie temperature and the spin and orbital magnetic moments change with Co concentration.

At first, we analyze the concentration dependence of MAE of the hexa-(Fe,Co)<sub>3</sub>C phase, see Fig. 4(a) and

Table III. We observe both positive and negative MAE values, indicating uniaxial and in-plane magnetocrystalline anisotropies, respectively. The highest MAE of 1.07 MJ m<sup>-3</sup> was obtained for a concentration of 20% Co, and the minimum MAE of -1.46 MJ m<sup>-3</sup> for 70% Co. This trend is not surprising, as an analogous course of MAE(*x*) with a positive maximum and a negative minimum was observed for the mentioned before (Fe<sub>1-x</sub>Co<sub>x</sub>)<sub>2</sub>B and (Fe<sub>1-x</sub>Co<sub>x</sub>)<sub>16</sub>C alloys [87, 88]. As argued in the indicated works on uniaxial alloys, the course of the MAE(*x*) relationship is due to the filling of the valence band of the alloy as the Co concentration increases. Since MAE is a subtle quantity that depends on the details of the band structure in the close vicinity of the Fermi level, an increase in valence band filling by even about 0.1 electron per atom can lead to significant changes in MAE.

For ortho-(Fe,Co)<sub>3</sub>C alloys, the Co concentration range is divided into regions: from 0% to 35%, from 35% to 75%, and from 75% to 100%, with the directions of magnetic easy axes [010], [001], and [100], respectively, see Fig. 4(b). The highest MAE value of 0.82 MJ m<sup>-3</sup> was obtained for a concentration of 90% Co. The course of MAE(*x*) clearly differs from the result for the hexagonal phase (Fe,Co)<sub>3</sub>C and the mentioned tetragonal phases Fe-Co-B. This is due, among other things, to the presence of three main crystallographic axes, where each of them can be an easy axis with a positive MAE value. On the other hand, the details of the MAE(*x*) waveform itself are due, as we mentioned above, to the gradual filling of the valence band as the Co concentration increases. Additionally, for orthorhombic alloys, we show the energy difference between two higher energies (DE<sub>32</sub> = E<sub>3</sub> - E<sub>2</sub>) complementing the MAE. The low DE<sub>32</sub> values, as observed for Co-rich phases, strengthen the uniaxial character of the magnetocrystalline anisotropy of these systems.

Unfortunately, there is no systematic study of the course of the magnetocrystalline anisotropy constant on Co concentration in (Fe,Co)<sub>3</sub>C alloys to verify our theoretical predictions. From scattered information, we learn that Choe *et al.* obtained for the powder ortho-Fe<sub>3</sub>C sample an MAE equal to 0.405 MJ m<sup>-3</sup> at 5 K [20]. Wu *et al.* synthesized a melt-spun sample of Fe<sub>2</sub>CoC and measured the MAE for it at 10 K as 0.96 MJ m<sup>-3</sup> [17]. However, their analysis showed the presence of about 10% by weight of the bcc Fe phase in the Fe<sub>2</sub>CoC sample [17], which can affect the anisotropy constant. In contrast, our calculations for about 1/3 Co concentration indicate MAE close to zero.

A feature of our MAE calculations is that they are made for a perfect monocrystal at 0 K, and modeling chemical disorder with VCA leads to overestimation of MAE. However, the trends thus predicted turned out to be in line with experimental results [87]. The anisotropy constant of real samples can be significantly affected by numerous additional factors. In addition to the role of temperature, in the case of (Fe,Co)<sub>3</sub>C alloys we are faced with the chemical instability of the phase, the presence of microstructure and extraneous phases in the samples,



and in the case of nanoparticles, the influence of nanostructuring. Given the complexity of the problem, the calculated MAEs for monocrystals at 0 K are a good starting point for understanding the relationships governing doping, and the MAE values obtained from the calculations are promising from an application point of view and encourages further exploration of magnetically hard materials in the cementite family.

The total spin magnetic moment ( $m_s$ ) is highest for the terminal  $\text{Fe}_3\text{C}$  phases for both hexagonal and orthorhombic structures, and decrease with Co concentration, see Figs. 4(c,d). We do not observe a pronounced maximum in the intermediate range. This behavior is similar to that observed, for example, for Fe/Co monoborides [68, 89]. The observed trend has to do with an increase in the number of electrons per atom with an increase in the concentration of Co in the system. Additional electrons from Co atoms fill the valence band, especially the  $3d$  orbitals, see Fig. 2. Since the majority Fe  $3d$  spin channels are almost completely occupied, additional electrons fill the minority  $3d$  spin channels, which reduces the occupancy difference between the spin channels, which is what defines the spin magnetic moment.

For  $(\text{Fe},\text{Co})_3\text{C}$  alloys, we observe significant differences in the total orbital magnetic moments ( $m_l$ ) determined for various crystallographic directions, see Figs. 4(e,f). Although in some cases orbital moment differences correlate with magnetocrystalline anisotropy, this time we do not observe such relation. The calculated orbital magnetic moments, see Table III, on the Fe sites of  $0.04\text{--}0.05 \mu_B$  are close to the value calculated for bcc Fe of  $0.045 \mu_B$  [82]. However, both calculated values underestimate the experimental orbital magnetic moment in bcc Fe of  $0.086 \mu_B$  [90]. The  $m_l$  values calculated for  $\text{Co}_3\text{C}$  phases are lower than the corresponding values for  $\text{Fe}_3\text{C}$  phases. Moreover, the  $m_l$  values determined for  $\text{Co}_3\text{C}$  are lower than the values for fcc Co of  $0.071 \mu_B$  [84]) and  $0.073 \mu_B$  [82].

Hexagonal  $(\text{Fe},\text{Co})_3\text{C}$  alloys with Co concentration from 0 to 30% are magnetically semi-hard, see Fig. 4(g). For negative values of MAE, seen in the center of the concentration range, we assumed  $\kappa = 0$ , see Table III. The hexagonal carbide with 90% Co indicates  $\kappa = 1.13$ , which defines it as magnetically hard. For orthorhombic alloys, see Fig. 4(h), semi-hard magnetic properties are observed for most of Co concentrations.

In the previous section, we discussed the Curie temperature results for the stoichiometric compounds. The calculated mean-field Curie temperatures were 1040 K for hexa- $\text{Fe}_3\text{C}$ , 310 K for hexa- $\text{Co}_3\text{C}$ , 570 K for ortho- $\text{Fe}_3\text{C}$ , and 458 K for ortho- $\text{Co}_3\text{C}$ . In Fig. 5, we show the courses of calculated  $T_C$  as a function of Co concentration. For hexa- $(\text{Fe},\text{Co})_3\text{C}$  phase, the relation is close to linear, while for the ortho- $(\text{Fe},\text{Co})_3\text{C}$  phase a maximum around 20% Co is visible. The close to linear relationship resembles the analogous experimental results for  $(\text{Fe},\text{Co})\text{B}$  and  $(\text{Fe},\text{Co})_2\text{B}$  alloys [89, 91], and the maximum in  $T_C$  resembles results for bcc FeCo alloys [92]. As in the discussed trends for MAE and magnetic moment,

the trends for  $T_C$  depend primarily on the valence band filling of the systems under study increasing with Co concentration, see also Ref. [93]. As experiments for ortho- $\text{Co}_3\text{C}$  nanoparticles have shown [24–27], we expect that for ortho- $(\text{Fe},\text{Co})_3\text{C}$  nanoparticles as well, Curie temperatures should be able to be raised to values above 500 K.

In summary, we calculated the basic magnetic properties for hexa- and ortho- $(\text{Fe},\text{Co})_3\text{C}$  alloys. Hexagonal alloys show a number of promising magnetic properties, such as a high Curie temperature of 1040 K for hexa- $\text{Fe}_3\text{C}$ , and a magnetic hardness ( $\kappa$ ) of 0.83 for hexa- $(\text{Fe}_{0.8}\text{Co}_{0.2})_3\text{C}$ . Nevertheless, their experimental synthesis has so far presented great difficulties, as explained by the positive formation energies of hexa- $\text{Fe}_3\text{C}$  and hexa- $\text{Co}_3\text{C}$  compounds, above those for corresponding orthorhombic phases. On the other hand, it has been experimentally proven that the ortho- $(\text{Fe},\text{Co})_3\text{C}$  phase is stabilizable. DFT calculations predict for it decrease of spin magnetic moment with Co concentration, and maximum in Curie temperature at about 20% Co. Experimental Curie temperatures determined for orthorhombic  $(\text{Fe},\text{Co})_3\text{C}$  nanoparticles of more than 500 K offer hope for the practical application of these alloys. Experiments also showed Curie temperature dispersion for ortho- $\text{Co}_3\text{C}$  nanoparticles, suggesting a strong effect of structuring on the magnetic properties of the system, including magnetic moment, magnetocrystalline anisotropy and Curie temperature. Most probably due to this feature, the MAE calculated here for ortho- $(\text{Fe},\text{Co})_3\text{C}$  alloys differ significantly from experimental data. However, at the same time, calculations and experiments indicate for selected ortho- $(\text{Fe},\text{Co})_3\text{C}$  compositions the promising MAE values of about  $1.0 \text{ MJ m}^{-3}$  at low temperatures, indicating the possibility of optimizing the alloys to reach similar values above room temperature. Mentioned optimization would consist of selecting proper Fe/Co ratio, nanoparticle size, and additions of other transition metal elements. The presence of Co in the alloy is, however, not advantageous from an economic point of view, so alloys with a high Co content are unlikely for applications requiring large amounts of material.

### III.3. $\text{Fe}_3\text{C}$ and $\text{Co}_3\text{C}$ alloys with transition metals

In this section, we will discuss calculation results for  $\text{Fe}_3\text{C}$  and  $\text{Co}_3\text{C}$  alloys with transition metals. In our models, the transition metal atom replaces one of the twelve Fe (or Co) atoms in the  $\text{Fe}_{11}\text{X}_1\text{C}_4$  (or  $\text{Co}_{11}\text{X}_1\text{C}_4$ ) supercell, see Fig. II. Similar models of ortho- $\text{Fe}_{11}\text{X}_1\text{C}_4$  alloys have been investigated by Shein *et al.* [37]. Below we will present the results of calculations of formation energies, magnetic moments, and magnetocrystalline anisotropy energies. These results are further complemented by Curie temperature calculations performed using the disorder local moments (DLM) method. In the following analysis, we consider hexa- $\text{Fe}_3\text{C}$ , ortho- $\text{Fe}_3\text{C}$ , and ortho- $\text{Co}_3\text{C}$  alloys, ignoring hexa- $\text{Co}_3\text{C}$  alloys. The decision to exclude hexa- $\text{Co}_3\text{C}$  alloys is due to the un-

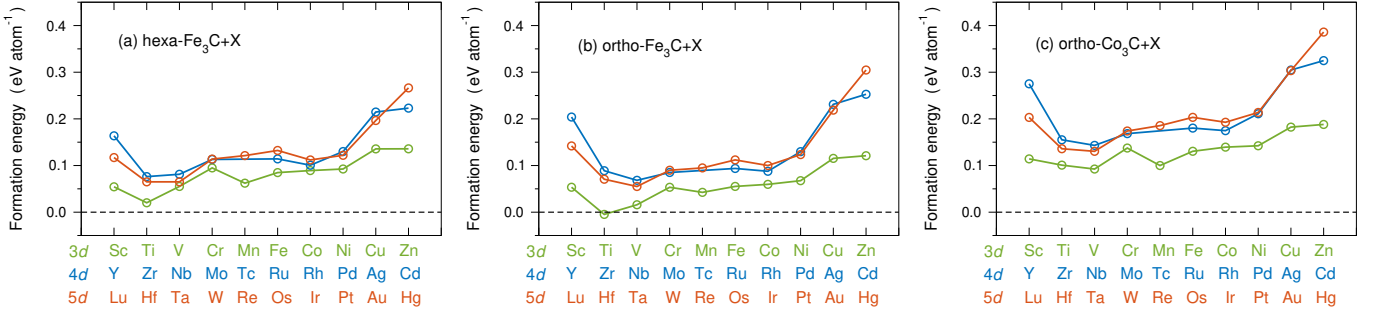


FIG. 6. Formation energies for (a) hexa- $\text{Fe}_3\text{C}$ , (b) ortho- $\text{Fe}_3\text{C}$ , and (c) ortho- $\text{Co}_3\text{C}$  alloys with  $3d$ ,  $4d$ , and  $5d$  transition metals  $X$  [ $(\text{Fe}/\text{Co})_{11}\text{X}_1\text{C}_4$ ]. The calculations were performed with FPLO18 code using the PBE functional and supercell approach.

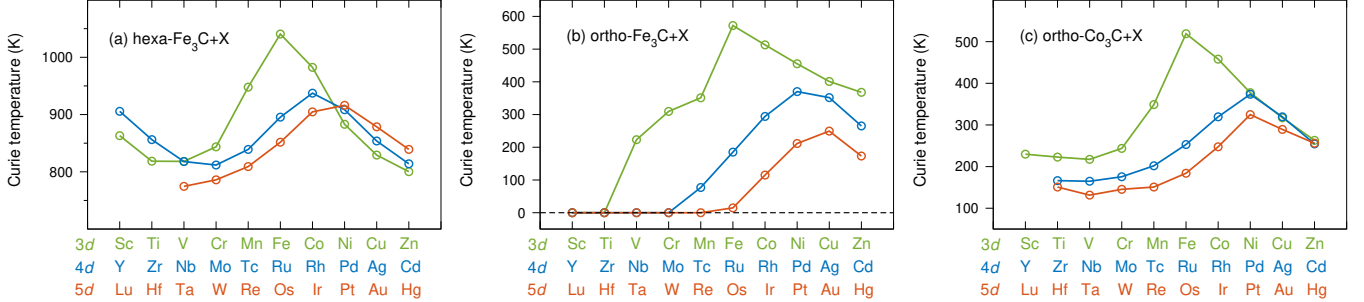


FIG. 7. The mean-field-theory Curie temperatures ( $T_C^{\text{MFT}}$ ) for hexa- and ortho- $(\text{Fe}_{0.916}\text{X}_{0.084})_3\text{C}$  alloys with  $3d$ ,  $4d$ , and  $5d$  transition metals  $X$ . The results were calculated using the FPLO5 code and the Perdew and Wang (PW92) functional. The chemical disorder was modeled with coherent potential approximation (CPA) and the paramagnetic state with disorder local moment (DLM-CPA) method.

promising properties of the hexa- $\text{Co}_3\text{C}$  compound (magnetic hardness equal zero and formation energy higher than for ortho- $\text{Co}_3\text{C}$  phase).

### III.3.1. Formation energy

Figure 6 presents the calculated formation energies for hexa- $\text{Fe}_3\text{C}$ , ortho- $\text{Fe}_3\text{C}$ , and ortho- $\text{Co}_3\text{C}$  alloys with transition metals. With one exception (ortho- $\text{Fe}_{11}\text{Ti}_1\text{C}_4$ ), all alloys have positive formation energies, implying lack of chemical stability. The positive values are in most cases relatively small, making it possible to stabilize the materials by forming nanoparticles, alloys, or composites [17, 21, 31, 49].

The plots of dependencies of formation energies on  $3d$  and  $4d$  transition metal substitutions in ortho- $\text{Fe}_3\text{C}$  are almost identical to the previously mentioned theoretical results [37, 54]. Although the formation energies of the alloys studied provide valuable information, the idealized single-phase nature of the models means that the actual impact of additives is best verified experimentally. Bulk ortho- $\text{Fe}_3\text{C}$  has been tested by Umemoto *et al.* [31], who found that Cr, Mn, V and Mo additions stabilize the cementite, whereas Ti, Ni, and Si destabilize it. Furthermore, it has been determined that the substitution of 5 at.% Ti leads to the appearance of additional phases of TiC and  $\alpha\text{-Fe}$  [31]. The formation energies of ortho- $\text{Co}_3\text{C}$  alloys are higher than those of ortho- $\text{Fe}_3\text{C}$ , however, still

relatively low.

### III.3.2. Curie temperature

In Fig. 7 we present the mean-field theory Curie temperatures ( $T_C^{\text{MFT}}$ ) calculated for hexa- $(\text{Fe}_{0.916}\text{X}_{0.084})_3\text{C}$ , ortho- $(\text{Fe}_{0.916}\text{X}_{0.084})_3\text{C}$ , and ortho- $(\text{Co}_{0.916}\text{X}_{0.084})_3\text{C}$  alloys with transition metals  $X$ . The transition metal concentration of 0.084 was chosen to reproduce the  $\frac{1}{12}$  concentration of transition metal element  $X$  in  $\text{Fe}_{11}\text{X}_1\text{C}_4$  models.

In Fig. 7 we see, that the dependencies of  $T_C$  on the atomic number of substitution have a clear sinusoidal trend and that each substitution reduces the  $T_C$  of the parental hexa- $\text{Fe}_3\text{C}$  compound. Nevertheless, all the considered hexa- $\text{Fe}_3\text{C} + \text{X}$  alloys show relatively high  $T_C$ .

Calculated trends for transition metal elements suggest that all substitutions, except Co, will significantly reduce the  $T_C$  of the alloy. Whereas, the elements  $4d$  and  $5d$  will have stronger effect than the elements  $3d$ . The transition metal elements on the left side of the periods reduce  $T_C$  to zero, which means the absence of magnetic ordering. Previous experiments confirm the reduction of Curie temperature after alloying of cementite with Cr, Mn, or Mo [29, 30]. However, it has been measured that up to about 2% Ni raises the Curie temperature of the cementite [29]. The effect of lowering  $T_C$  can make it difficult or impossible to use most transition metals as

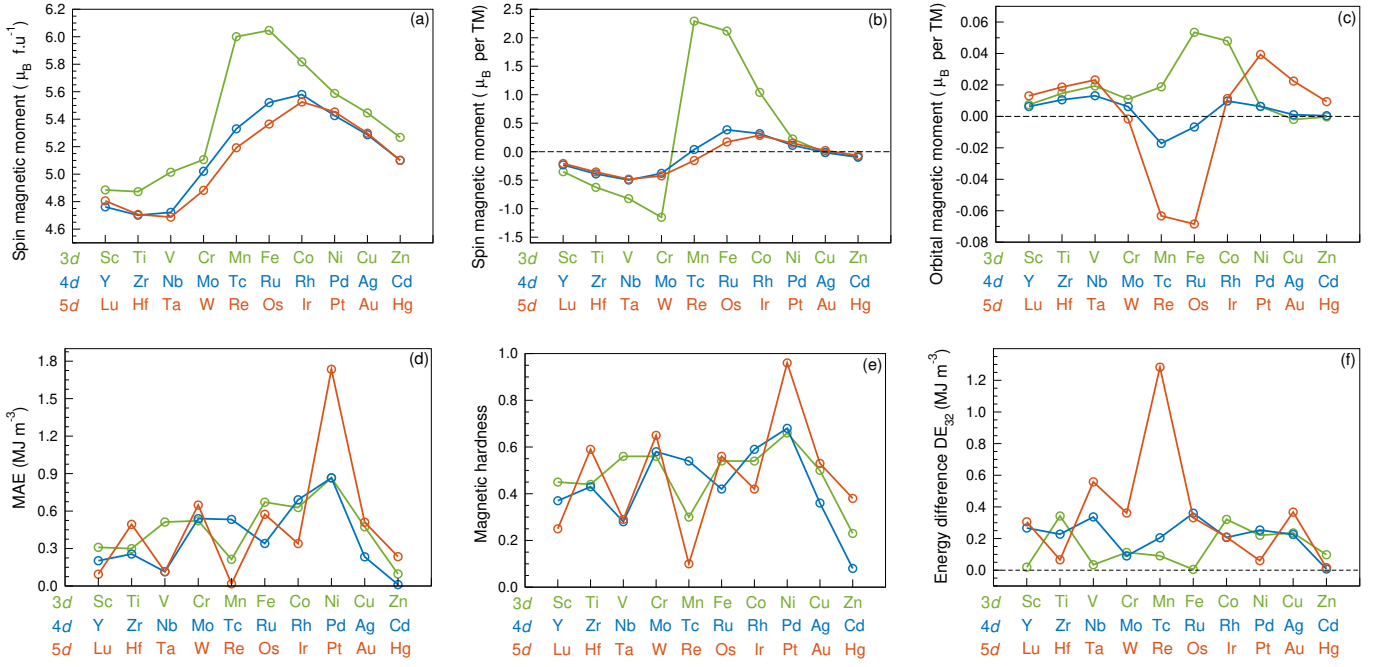


FIG. 8. The magnetic properties of hexa- $\text{Fe}_3\text{C}$  alloys with 3d, 4d, and 5d transition metals X ( $\text{Fe}_{11}\text{X}_1\text{C}_4$ ): (a) total spin magnetic moment (per formula unit); (b, c) spin and orbital magnetic moments on substitution atoms X (per TM atom); (d) magnetocrystalline anisotropy energy (MAE); (e) magnetic hardness; and (f) energy difference ( $\text{DE}_{32}$ ) between the two higher energies among the three total energies calculated along the three main crystallographic axes. The calculations were performed with FPLO18 code using the PBE functional and supercell approach.

additives to affect MAE and magnetic hardness. The solution could be, for example, a combination of transition metal alloying on the Fe site with B alloying on the C side. Indeed, the experiment showed a linear growth in  $T_C$  up to 851 K with increasing B concentration in ortho- $\text{Fe}_3(\text{B,C})$  borocarbides [21].

Calculations indicate that only Fe substitution raises the  $T_C$  of the ortho- $\text{Co}_3\text{C}$ -based system, while all other elements considered lower it. The determined  $T_C$  values below and well below 400 K suggest the impossibility of using most ortho- $\text{Co}_3\text{C} + \text{X}$  alloys as permanent magnets. The solution, as we suggested above, could be the alloying of B at the C position, since, as shown experimentally, the  $T_C$  of ortho- $\text{Co}_3\text{B}$  is much higher than the value for ortho- $\text{Co}_3\text{C}$  and is 750 K [16].

### III.3.3. Magnetic moments and magnetic hardness

After discussing the formation energy and Curie temperature, we will show how alloying with transition metals affect the magnetic moments and magnetic hardness, see Figs. 8, 9, and 10 for hexa- $\text{Fe}_{11}\text{X}_1\text{C}_4$ , ortho- $\text{Fe}_{11}\text{X}_1\text{C}_4$ , and ortho- $\text{Co}_{11}\text{X}_1\text{C}_4$  alloys, respectively. In the majority of instances, clear patterns emerge with regard to the dependencies. Trends in magnetic moments are similar to those calculated previously for alloys of ortho- $\text{Fe}_3\text{C}$  [37],  $\text{CeFe}_{12}$  [85], monoborides [68], and Fe [94–96]. MAE trends, on the other hand, do not resemble previous findings.

#### III.3.3.1. Hexa- $\text{Fe}_3\text{C}$ alloys with transition metals

We will begin our discussion of the results with hexa- $\text{Fe}_3\text{C}$  alloys. Figure 8 presents a collection of the magnetic properties for alloys with 3d, 4d and 5d metals. The spin magnetic moment trends for the three series of transition metals have a waveform shape, see Figs. 8(a,b). The parent system without substitution, hexa- $\text{Fe}_3\text{C}$ , shows the highest total spin magnetic moment. All transition metal substitutions are spin polarized in the ferromagnetic medium and contribute to the total magnetic moment of the alloy, lowering its value. The orbital magnetic moments on the substitution sites are much smaller from spin magnetic moments, and oscillate between  $-0.07$  and  $+0.06 \mu_B \text{ atom}^{-1}$ , see Fig. 8(c).

Figures 8(d) and 8(f) show the magnetocrystalline anisotropy energies (MAE and  $\text{DE}_{32}$ ) for hexa- $\text{Fe}_{11}\text{X}_1\text{C}_4$  alloys. From all considered compositions, the system with Pt has the highest MAE of  $1.73 \text{ MJ m}^{-3}$ . This value corresponds to the highest magnetic hardness of 0.96, see Fig. 8(e). Our previous results for transition metal alloying in the Fe matrix, also pointed to Pt as a metal that stands out for its exceptionally positive effect on MAE [96]. Unfortunately, the high price of platinum, is not in favor of potential applications.

#### III.3.3.2. Ortho- $\text{Fe}_3\text{C}$ alloys with transition metals

Trends of magnetic moments for ortho- $\text{Fe}_3\text{C}$  alloys with transition metal elements, see Fig. 9(a-c), are similar to those presented above for hexa- $\text{Fe}_3\text{C}$  alloys. However, the values of total spin magnetic moments are lower by about

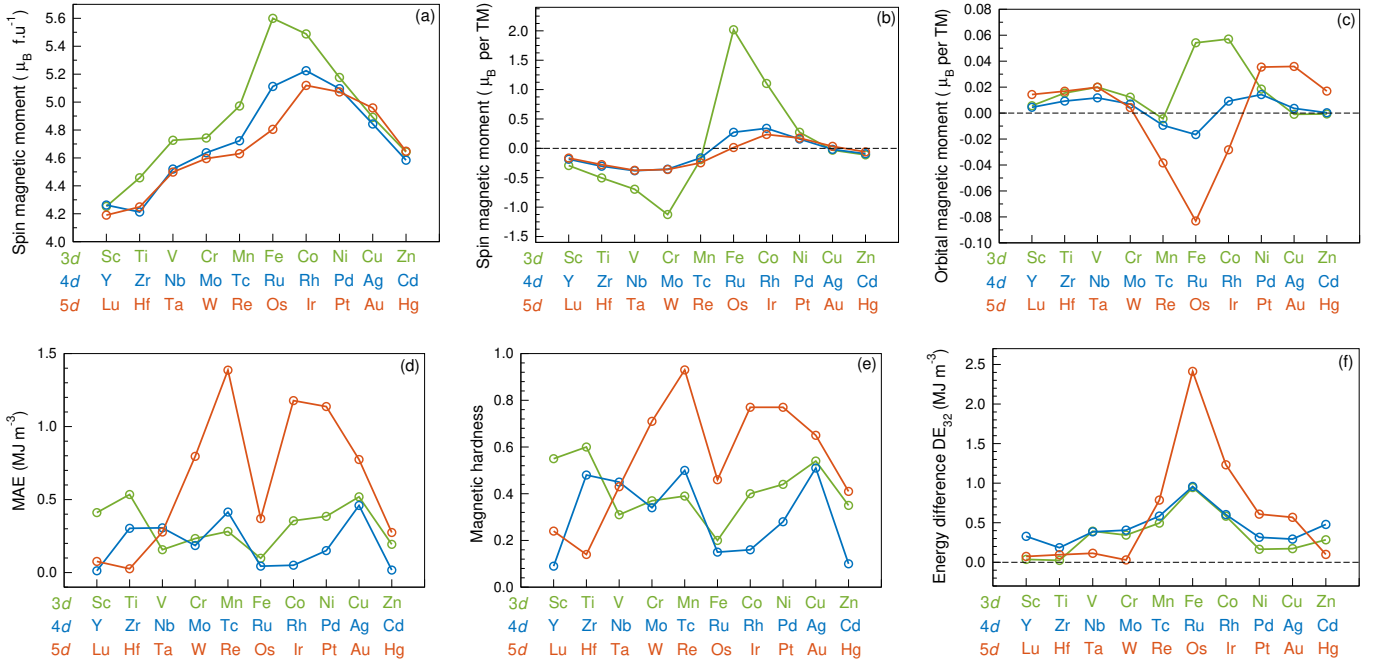


FIG. 9. The magnetic properties of ortho- $\text{Fe}_3\text{C}$  alloys with  $3d$ ,  $4d$ , and  $5d$  transition metals  $X$  ( $\text{Fe}_{11}\text{X}_1\text{C}_4$ ): (a) total spin magnetic moment (per formula unit); (b, c) spin and orbital magnetic moments on substitution atoms  $X$  (per TM atom); (d) magnetocrystalline anisotropy energy (MAE); (e) magnetic hardness; and (f) energy difference ( $\text{DE}_{32}$ ) between the two higher energies among the three total energies calculated along the three main crystallographic axes. The calculations were performed with FPLO18 code using the PBE functional and supercell approach.

$0.5 \mu_{\text{B}} \text{f.u.}^{-1}$ . Similar trends in local magnetic moments on transition metal substitutions were also observed in previous calculations for ortho- $\text{Fe}_{11}\text{X}_1\text{C}_4$  alloys with  $3d$  and  $4d$  elements [37]. Among the ortho- $\text{Fe}_{11}\text{X}_1\text{C}_4$  alloys, the parent ortho- $\text{Fe}_3\text{C}$  compound has the highest total spin magnetic moment of  $5.60 \mu_{\text{B}} \text{f.u.}^{-1}$ .

The MAE and magnetic hardness of ortho- $\text{Fe}_3\text{C}$  alloys appear more promising than that of hexa- $\text{Fe}_3\text{C}$  alloys, see Fig. 9(d,e). The MAE increases above  $1 \text{ MJ m}^{-3}$  for Re, Ir, and Pt substitutions, leading to MAE values of  $1.4$ ,  $1.2$ , and  $1.1 \text{ MJ m}^{-3}$ , respectively. However, as shown in Fig. 9(e), none of the alloys can be classified as a hard magnetic ( $\kappa > 1$ ). The magnetic hardness closest to exceeding unity ( $0.93$ ) has an alloy with Re. In addition, as we showed earlier, alloying ortho- $\text{Fe}_3\text{C}$  with  $5d$  transition metals leads to a strong decrease in Curie temperature. It makes the system with Re ultimately not a good candidate for a permanent magnet either.

In systems (such as orthorhombic) that do not have a unique distinguished crystallographic axis, we must be careful when considering MAE values, checking  $\text{DE}_{32}$ , see Sec. II for definition. The  $\text{DE}_{32}$  equal to  $0.8 \text{ MJ m}^{-3}$  for ortho- $\text{Fe}_{11}\text{Re}_1\text{C}_4$  with MAE of  $1.4 \text{ MJ m}^{-3}$  suggests uniaxial magnetocrystalline anisotropy. On the other hand,  $\text{DE}_{32}$  of around  $2.4 \text{ MJ m}^{-3}$  for ortho- $\text{Fe}_{11}\text{Os}_1\text{C}_4$ , compared to MAE of  $0.4 \text{ MJ m}^{-3}$  suggests magnetocrystalline anisotropy close to easy-plane.

### III.3.3.3. Ortho- $\text{Co}_3\text{C}$ alloys with transition metals

The magnetic hardness of the ortho- $\text{Co}_3\text{C}$  is one of

the highest among the considered orthorhombic compositions, see Fig. 4. The magnetic properties calculated for ortho- $\text{Co}_3\text{C}$  alloys are shown in Fig. 10. For the total spin magnetic moment, see Fig. 10(a), we observe sinusoidal behavior, like before for hexa- $\text{Fe}_3\text{C}$  alloys. However, the total magnetic moments calculated for ortho- $\text{Co}_3\text{C}$  alloys are about half those for  $\text{Fe}_3\text{C}$  alloys. The maximum of spin magnetic moment, for  $\text{Co}_{11}\text{Mn}_1\text{C}_4$ , is equal to  $3.4 \mu_{\text{B}}$  per f.u. and the minimum, for  $\text{Co}_{11}\text{W}_1\text{C}_4$ , is equal to  $2.2 \mu_{\text{B}}$  per f.u. Only for Mn and Fe substitutions, the spin magnetic moment is higher than for Co in the initial ortho- $\text{Co}_3\text{C}$  phase, see Fig. 10(b). The orbital magnetic moments on the substituted sites, ranging from  $-0.04$  to  $+0.04 \mu_{\text{B}} \text{atom}^{-1}$ , are also about twice smaller than in the case of  $\text{Fe}_3\text{C}$  alloys, see Fig. 10(c).

In Figure 10(d), we see once again that the MAE significantly depends on the substituting element. The calculated MAE results take a range from zero to  $0.8 \text{ MJ m}^{-3}$ . The MAE and magnetic hardness calculations indicate that  $\text{Co}_{11}\text{W}_1\text{C}_4$  and  $\text{Co}_{11}\text{Os}_1\text{C}_4$  can be classified as hard magnetic ( $\kappa > 1$ ) with MAE values equal to  $0.5$  and  $0.8 \text{ MJ m}^{-3}$ , respectively, see Figs. 10(d,e). Unfortunately, as for ortho- $\text{Fe}_3\text{C} + X$  alloys,  $5d$  substitutions will strongly lower the Curie temperature, making their use impractical. Alloying of ortho- $\text{Co}_3\text{C}$  with transition metals in most cases causes a decrease in magnetic hardness. The small increase in magnetic hardness predicted for alloying with W and Os is burdened by the high prices of these elements and expected significant decrease in Curie temperature.



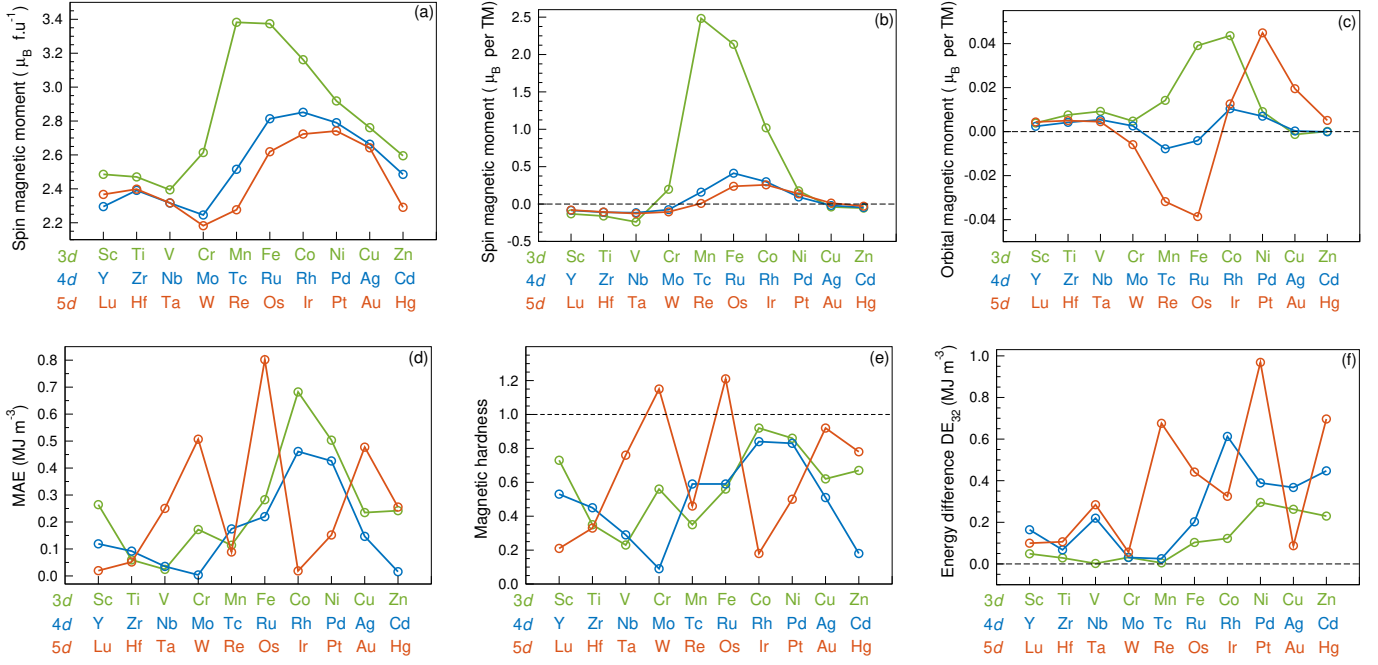


FIG. 10. The magnetic properties of ortho- $\text{Co}_3\text{C}$  alloys with  $3d$ ,  $4d$ , and  $5d$  transition metals  $X$  ( $\text{Co}_{11}\text{X}_1\text{C}_4$ ): (a) total spin magnetic moment (per formula unit of two atoms); (b, c) spin and orbital magnetic moments on substitution atoms  $X$  (per TM atom); (d) magnetocrystalline anisotropy energy (MAE); (e) magnetic hardness; and (f) energy difference ( $\text{DE}_{32}$ ) between the two higher energies among the three total energies calculated along the three main crystallographic axes. The calculations were performed with FPLO18 code using the PBE functional and supercell approach.

In summary, calculations of Curie temperature and magnetic hardness do not suggest that alloying with transition metals of hexa- $\text{Fe}_3\text{C}$ , ortho- $\text{Fe}_3\text{C}$ , and ortho- $\text{Co}_3\text{C}$  compounds lead to a significant improvement in their potential for permanent magnet applications. The magnetic hardness of hexa- $\text{Fe}_3\text{C} + X$  alloys, except for Pt substitution, does not exceed 0.7, and in addition, the formation energies of hexagonal alloys are higher than those of orthorhombic alloys, making them difficult to obtain. In the case of ortho- $\text{Fe}_3\text{C} + X$  alloys, Re, Ir, and Pt lead to an increase in magnetic hardness but at the same time lower the Curie temperature to values far below room temperature, which disqualifies potential applications for permanent magnets. In the case of the most promising hard magnetic ortho- $\text{Co}_3\text{C}$  compound, a few  $5d$  transition metals (Re, Pt, Au) do lead to a slight increase in magnetic hardness, but at the price of a significant drop in Curie temperature.

### III.4. $(\text{Fe},\text{Co})_3(\text{B},\text{C},\text{N})$ alloys

In Sec. III.2 we discussed  $(\text{Fe}/\text{Co})_3\text{C}$  alloys in which substituting takes place at the  $3d$  sites (Fe and Co). An additional degree of freedom in controlling the composition of  $\text{Fe}_3\text{C}$ -type alloys is substituting at the  $2p$  (carbon) site [21, 57, 97]. Two natural candidates for such alloying are boron and nitrogen – carbon’s neighbors in the periodic table. Although  $\text{Fe}_3(\text{B},\text{C})$  borocarbides have been synthesized since at least the 1950s [21], they have not re-

TABLE V. Magnetocrystalline anisotropy energy [MAE ( $\text{MJ m}^{-3}$ )] and magnetic hardness [ $\kappa$ ] of selected  $(\text{Fe},\text{Co})_3(\text{B},\text{C},\text{N})$  compositions with hexagonal and orthorhombic symmetries calculated with FPLO18 code using PBE functional and virtual crystal approximation to model alloying.

Compound/Alloy	Hexagonal		Orthorhombic	
	MAE	$\kappa$	MAE	$\kappa$
$\text{Fe}_3\text{B}$	0.05	0.18	0.53	0.50
$\text{Fe}_3\text{C}$	0.68	0.63	0.11	0.21
$\text{Fe}_3\text{N}$	-0.25	0	0.55	0.45
$\text{Co}_3\text{B}$	-0.09	0	0.16	0.41
$\text{Co}_3\text{C}$	-0.15	0	0.67	0.91
$\text{Co}_3\text{N}$	-0.15	0	0.82	0.92
$\text{Co}_3(\text{C}_{0.3}\text{N}_{0.7})$	–	–	0.83	1.02
$\text{Co}_3(\text{B}_{0.4}\text{C}_{0.6})$	0.47	1.01	–	–
$(\text{Fe}_{0.1}\text{Co}_{0.9})_3\text{C}$	0.75	1.13	–	–
$(\text{Fe}_{0.1}\text{Co}_{0.9})_3(\text{C}_{0.9}\text{N}_{0.1})$	0.69	1.10	–	–
$(\text{Fe}_{0.7}\text{Co}_{0.3})_3(\text{B}_{0.7}\text{C}_{0.3})$	1.19	0.91	–	–

ceived wider attention. However, replacing carbon with boron in  $\text{Fe}_3(\text{B},\text{C})$  alloys leads to significant changes in properties. Nicholson showed experimentally that in the alloys range from  $\text{Fe}_3\text{C}$  to  $\text{Fe}_3\text{B}$ , the magnetic moment grows by about 10% and the Curie temperature linearly increases from 481 K to the impressive 824 K [21]. A similar significant increase in Curie temperature during

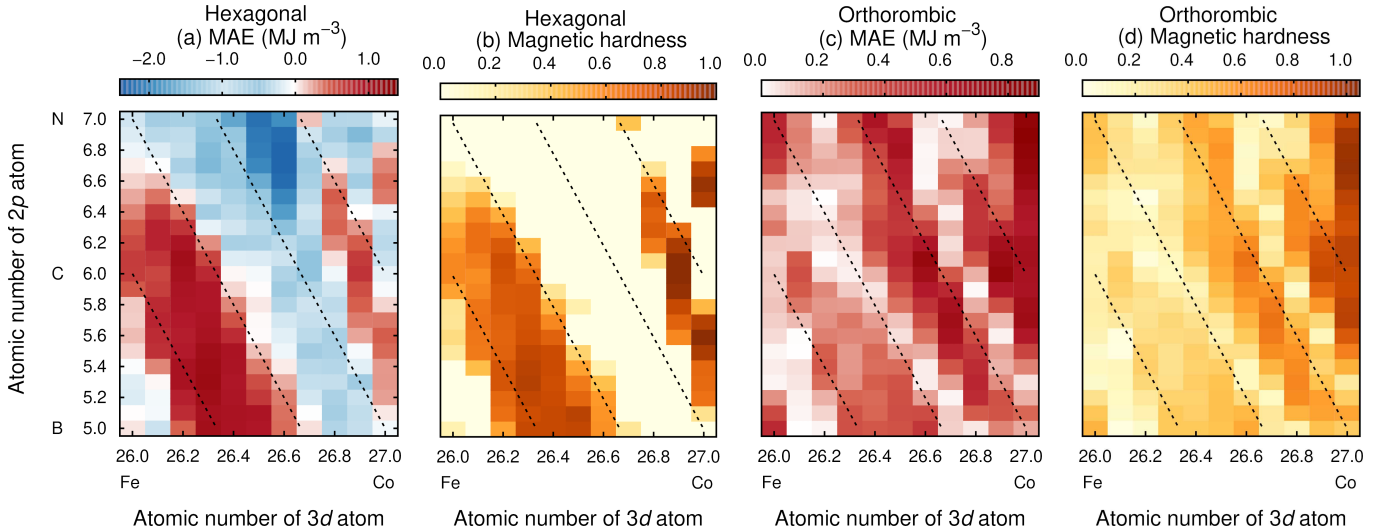


FIG. 11. (a,c) Magnetocrystalline anisotropy energy and (b,d) magnetic hardness as dependencies on the average atomic number of the elements  $3d$  and  $2p$  calculated for hexagonal and orthorhombic phase of  $(\text{Fe,Co})_3(\text{B,C,N})$  pseudobinary alloys. Calculations performed with virtual crystal approximation (VCA), using the FPLO18 code with PBE exchange-correlation potential. Along the dashed isolines, the total atomic number per formula (and thus the total number of electrons per formula) is constant.

alloying at the  $p$ -site was also observed for the transition from  $\text{Fe}_5\text{PB}_2$  to  $\text{Fe}_5\text{SiB}_2$ , where an alloying element with one less atomic number was also used [98]. Medvedeva *et al.* have shown by supercell method that B alloying increases the magnetic moment of ortho- $\text{Fe}_3(\text{B,C})$  borocarbides and stabilizes them [57]. Ande and Sluiter, also using supercell calculations, tested the effect of substitution of Al, Si, P, or S at the C-site in ortho- $\text{Fe}_3\text{C}$  on the stability of solid solutions [54]. Moreover, the hexa- $\text{Fe}_3\text{N}$  nitride has a negative formation energy, hence it stabilizes the hexagonal nitrocarbides [33]. The hexa- $\text{Fe}_3(\text{C,N})$  powder consisting of 5% C was previously synthesized [33] and classified as magnetically soft.

In this section, we extend the study of  $(\text{Fe,Co})_3\text{C}$  alloys, and analyze the alloying at both the  $3d$  and  $2p$  sites within a single model. We consider  $(\text{Fe,Co})_3(\text{B,C,N})$  alloys with concentration range at  $3d$  site from Fe to Co (atomic numbers from 26 to 27) and at  $2p$  site from B, through C, to N (atomic numbers from 5 to 7). In Figure 11, we show maps of MAE and magnetic hardness for hexagonal and orthorhombic alloys. Furthermore, in Table V, we present calculated values of MAE and magnetic hardness for stoichiometric compounds and for alloys with the highest determined magnetic hardnesses.

Studying alloying simultaneously at  $3d$  and  $2p$  sites allows conclusions to be drawn about the basic nature of the MAE. Particularly noticeable in MAE maps are diagonal stripes, see Fig. 11. It means that the MAE does not depend on the details of the composition, but on the total atomic number of the system (or equivalent total number of electrons). The dependence of the MAE on the number of electrons is in agreement with the model of the origin of the MAE as a subtle property, which depends on the details of the valence band form and its filling level [87].

The hexagonal  $(\text{Fe,Co})_3(\text{B,C,N})$  system exhibit MAE from  $-2.4$  to  $1.19 \text{ MJ m}^{-3}$ , see Fig. 11. The highest value of MAE ( $1.19 \text{ MJ m}^{-3}$ ) is obtained for  $(\text{Fe}_{0.7}\text{Co}_{0.3})_3(\text{B}_{0.7}\text{C}_{0.3})$ . Several other compositions also exhibit magnetic hardness above unity, see Table V. Moreover, the orthorhombic  $(\text{Fe,Co})_3(\text{B,C,N})$  system shows only positive MAE values, while the direction of the magnetic easy axis changes. For orthorhombic phases, the highest values of magnetic hardness are observed for full Co content, agreeing with the previous results for  $(\text{Fe,Co})_3\text{C}$  alloys, see Fig. 4. The highest value of MAE ( $0.83 \text{ MJ m}^{-3}$ ; leading to magnetic hardness of 1.02) was determined for  $\text{Co}_3(\text{C}_{0.3}\text{N}_{0.7})$ . However, alloying with N can further destabilize orthorhombic carbides.

As we said, the most promising MAEs are observed for orthorhombic alloys with full Co content, see Fig. 11. To take a closer look at this range, in a one-dimensional Fig. 12 we again show the dependence of MAE on element concentration at the  $2p$  position, along with a plot of spin magnetic moment. At the center of B-C-N range is the ortho- $\text{Co}_3\text{C}$  compound, known from previous discussion as a promising composition for hard magnetic applications. Although raising the nitrogen concentration leads to an increase in MAE, for reasons related to the instability of the ortho- $\text{Co}_3\text{N}$  phase, a better approach may be to alloy ortho- $\text{Co}_3\text{C}$  with boron, which should both stabilize the system and raise its Curie temperature. Moreover, the dependence of the magnetic moment on the concentration of  $2p$  atoms is non-intuitive, see Fig. 12(b). While in the range from B to C it is qualitatively consistent with the ten percent decrease in magnetic moment measured for the isostructural  $\text{Fe}_3(\text{B,C})$  phase [21], in the range from C to N the spin magnetic moment shows a surprising minimum. It comes from the minima of spin magnetic moments at both non-equivalent

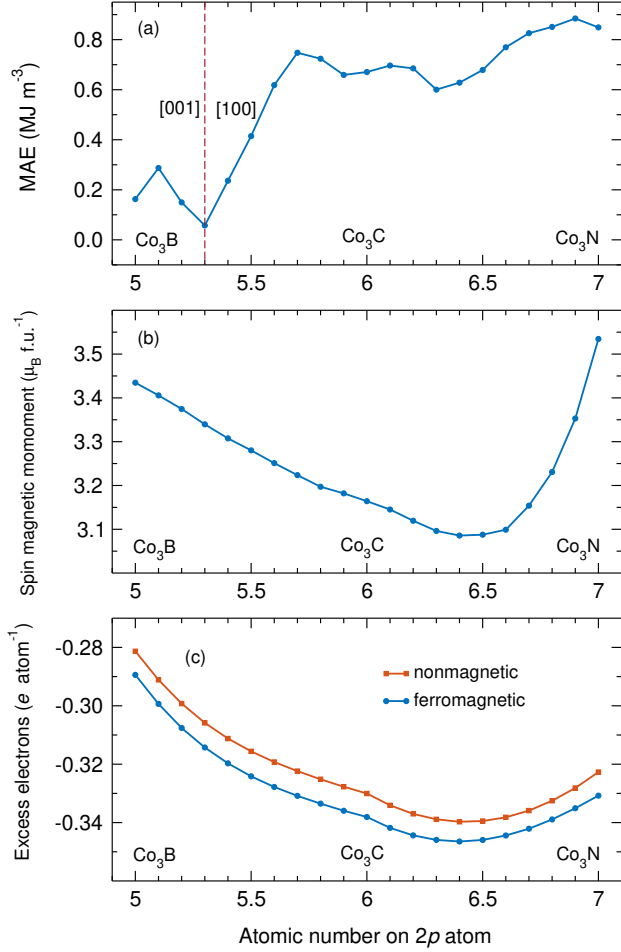


FIG. 12. The Magnetocrystalline anisotropy energy (a), total spin magnetic moment (b), and excess electrons at the Co site (c) as a function of the average atomic number of elements  $2p$  calculated for orthorhombic  $\text{Co}_3(\text{B,C,N})$  alloys. In the MAE plot, the red dashed line separates the regions with different directions of magnetic easy axis. Calculations were performed with virtual crystal approximation (VCA), using the FPLO18 code with PBE exchange-correlation potential.

Co positions. Light is shed on the minima in magnetic moments by density analysis, which in the case of the FPLO code involves determining the number of electrons in local density functions. The excess charge on Co atom relative to the neutral cobalt atom is shown in Fig. 12(c). The electrons from the cobalt atoms transfer to the  $2p$  atoms. The observed minimum in the magnetic moment correlates with the charge minimum. Additional calculations without spin polarization (non-magnetic) show that the charge minimum is primary to the magnetic moment. The theoretical minimum discussed here for the orthorhombic phase may not be experimentally verifiable, since experiments to date for  $\text{Co}_3\text{N}_{1+\delta}$  [99] and  $(\text{Fe,Co})_3\text{N}$  [100] indicate that  $\text{Co}_3\text{N}$  prefers the hexagonal structure.

Furthermore, the calculated MAE of  $\text{Co}_3\text{B}$  of less than  $0.2 \text{ MJ m}^{-3}$  is much lower than the corresponding room-temperature experimental value of  $0.65 \text{ MJ m}^{-3}$  [16].

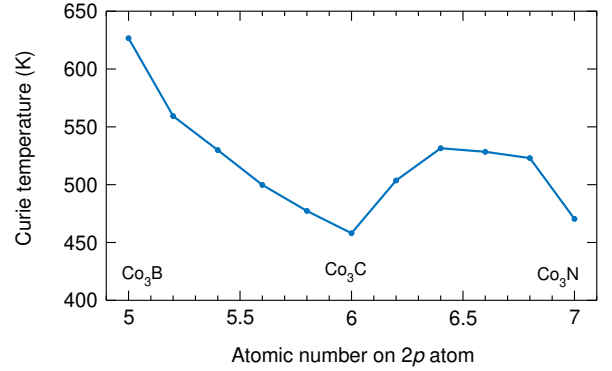


FIG. 13. The mean-field-theory Curie temperatures ( $T_C^{\text{MFT}}$ ) calculated for orthorhombic  $\text{Co}_3(\text{B,C,N})$  alloys as a function of the average atomic number of  $2p$  element. The results were calculated using the FPLO5 code and the Perdew and Wang (PW92) functional. The chemical disorder was modeled with coherent potential approximation (CPA) and the paramagnetic state with disorder local moment (DLM-CPA) method.

The discrepancy is due to, among other things, the dependence of MAE on temperature, as the calculations were performed at 0 K.

As we discussed earlier, the experimental Curie temperature values for ortho- $\text{Co}_3\text{C}$  were determined for nanoparticles and range from 498 K to 650 K [24–27] and are also significantly higher than the value for solid ortho- $\text{Fe}_3\text{C}$  of 481 K [21]. Mean-field theory calculations, which customarily overestimate the Curie temperature, give for ortho- $\text{Co}_3\text{C}$  a value of 458 K, suggesting that we should actually expect an experimental  $T_C$  about 300 K for ortho- $\text{Co}_3\text{C}$ . The experimental Curie temperatures of ortho- $\text{Co}_3\text{B}$  are between 710 K [76] and 750 K [16], much higher than for the isostructural carbide. In Fig. 13, we show the results of Curie temperature calculations in the ortho- $\text{Co}_3(\text{B-C-N})$  concentration range. In agreement with the experiment, we observe a decrease in Curie temperature with the transition from  $\text{Co}_3\text{B}$  to  $\text{Co}_3\text{C}$ . However, for the transition from  $\text{Co}_3\text{C}$  to  $\text{Co}_3\text{N}$ , we observe a maximum in the Curie temperature. A similar maximum in  $T_C$  was observed experimentally for  $\epsilon\text{-Fe-N}$  system with increasing nitrogen concentration [101]. As we mentioned above, since  $\text{Co}_3\text{N}$  seems to prefer the hexagonal phase, the presented  $T_C$  results for the ortho- $\text{Co}_3(\text{C-N})$  system will most probably remain only interesting theoretical considerations.

In summary, the alloying at the  $2p$  position, as discussed in this section, allows for the control of MAE, magnetic moment, and Curie temperature. Alloying the considered carbides with boron leads to an increase in the Curie temperature by several tens of percent. The increase in Curie temperature during alloying with boron correlates with an increase in magnetic moment up to about 10%. For the more stable orthorhombic phases, the highest magnetic hardnesses ( $\sim 0.9$ ) are found near the  $\text{Co}_3\text{C}$  composition, while remaining similarly high until about 30% boron alloying. Furthermore, the observation that MAE can depend on the total number of

electrons in the system can prove useful in the designing of new compositions of magnetically hard materials.

#### IV. SUMMARY AND CONCLUSIONS

In this study, we employed a first-principles approach to investigate the influence of composition on the magnetic properties of  $\text{Fe}_3\text{C}$ -type alloys. The objective was to identify alloys that exhibit enhanced magnetic hardness. This work has been divided into four parts. In the first, we have presented results for  $\text{Fe}_3\text{C}$  and  $\text{Co}_3\text{C}$  compounds, in the second for  $(\text{Fe},\text{Co})_3\text{C}$  alloys, in the third for  $\text{Fe}_3\text{C}$  and  $\text{Co}_3\text{C}$  alloys with transition metals, and in the fourth for  $(\text{Fe},\text{Co})_3(\text{B-C-N})$  alloys. In each instance, both hexagonal and orthorhombic structures were analyzed. For  $\text{Fe}_3\text{C}$  and  $\text{Co}_3\text{C}$  compounds, we examined what effect the form of the exchange-correlation potential has on the MAE and magnetic moment. By determining the dependence of the MAE on the fixed spin (magnetic) moment, we have preliminarily identified the range of MAE that the systems under consideration can adopt under varying temperatures or alloy compositions. The outcome of the investigation was not particularly encouraging. Of the four compounds considered, none proved to be magnetically hard. The highest magnetic hardness of 0.91 was predicted for ortho- $\text{Co}_3\text{C}$ . In order to investigate the magnetic properties of  $(\text{Fe},\text{Co})_3\text{C}$  alloys, we employed the virtual crystal approximation to calculate changes in magnetic properties as a function of Co concentration. This analysis led to the identification of magnetically hard Co-rich hexa- $(\text{Fe}_{0.1}\text{Co}_{0.9})_3\text{C}$  phase. Furthermore, we considered a series of hexa- $\text{Fe}_3\text{C}$ , ortho- $\text{Fe}_3\text{C}$ , and ortho- $\text{Co}_3\text{C}$  alloys with transition metals at a

concentration of 1/12 on Fe or Co site. Calculations of the Curie temperature and magnetic hardness do not indicate that alloying with transition metals increases their potential for permanent magnet applications. Finally, we found that a considerable proportion of the ortho- $\text{Co}_3(\text{B-C-N})$  alloys are magnetically hard, of which boron substitution raises the Curie temperature and improves stability.

The most universal result of this work is the interpretation of the two-dimensional dependence of MAE on concentration at both  $3d$  and  $2p$  positions of  $(\text{Fe-Co})_3(\text{B-C-N})$  alloys. The diagonal stripes visible in the MAE maps are interpreted as the dependence of MAE on the total number of electrons in the system, which is weakly responsive to the details of the occupancies at individual sites. This type of dependence offers a novel perspective on the design of compositions of hard magnetic materials.

#### ACKNOWLEDGMENTS

We acknowledge the financial support from the National Science Center of Poland under grants DEC-2019/35/O/ST5/02980 – PRELUDIUM BIS 1 (J.S.-A.) and DEC-2021/41/B/ST5/02894 – OPUS 21 (J.R.-G. and MW). Part of the calculation was made in the Poznan Supercomputing and Networking Centre (PSNC/PCSS). We thank P. Leśniak and D. Depcik for compiling the scientific software and managing the computer cluster at the Institute of Molecular Physics, Polish Academy of Sciences. We thank Z. Śniadecki and K. Synoradzki for reading the manuscript and providing valuable comments.

- 
- [1] O. Gutfleisch, M. A. Willard, E. Brück, C. H. Chen, S. G. Sankar, and J. P. Liu, Magnetic materials and devices for the 21st century: Stronger, lighter, and more energy efficient, *Adv. Mater.* **23**, 821 (2011).
  - [2] F. Ronning and S. Bader, Rare earth replacement magnets, *J. Phys.: Condens. Matter* **26**, 060301 (2014).
  - [3] L. H. Lewis and F. Jiménez-Villacorta, Perspectives on permanent magnetic materials for energy conversion and power generation, *Metall. Mater. Trans. A* **44**, 2 (2013).
  - [4] B. J. Smith, M. E. Riddle, M. R. Earlam, C. Iloeje, and D. Diamond, *Rare Earth Permanent Magnets: Supply Chain Deep Dive Assessment*, Tech. Rep. (USDOE Office of Policy, Washington DC (United States), 2022).
  - [5] K. Bourzac, The rare-earth crisis, *Technology Review* **114**, 58 (2011).
  - [6] M. D. Kuz'min, K. P. Skokov, H. Jian, I. Radulov, and O. Gutfleisch, Towards high-performance permanent magnets without rare earths, *J. Phys. Condens. Matter* **26**, 064205 (2014).
  - [7] K. P. Skokov and O. Gutfleisch, Heavy rare earth free, free rare earth and rare earth free magnets - vision and reality, *Scr. Mater.* **154**, 289 (2018).
  - [8] J. Cui, M. Kramer, L. Zhou, F. Liu, A. Gabay, G. Hadjipanayis, B. Balasubramanian, and D. Sellmyer, Current progress and future challenges in rare-earth-free permanent magnets, *Acta Mater.* **158**, 118 (2018).
  - [9] D. Li, Y. Li, D. Pan, Z. Zhang, and C.-J. Choi, Prospect and status of iron-based rare-earth-free permanent magnetic materials, *J. Magn. Magn. Mater.* **469**, 535 (2019).
  - [10] A. Vishina, O. Y. Vekilova, T. Björkman, A. Bergman, H. C. Herper, and O. Eriksson, High-throughput and data-mining approach to predict new rare-earth free permanent magnets, *Phys. Rev. B* **101**, 094407 (2020).
  - [11] J. M. D. Coey, Perspective and Prospects for Rare Earth Permanent Magnets, *Engineering* **6**, 119 (2020).
  - [12] Y. Zhang, G. S. Chaubey, C. Rong, Y. Ding, N. Poudyal, P.-c. Tsai, Q. Zhang, and J. P. Liu, Controlled synthesis and magnetic properties of hard magnetic  $\text{Co}_x\text{C}$  ( $x=2, 3$ ) nanocrystals, *J. Magn. Magn. Mater.* **323**, 1495 (2011).
  - [13] K. J. Carroll, Z. J. Huba, S. R. Spurgeon, M. Qian, S. N. Khanna, D. M. Hudgins, M. L. Taheri, and E. E. Carpenter, Magnetic properties of  $\text{Co}_2\text{C}$  and  $\text{Co}_3\text{C}$  nanoparticles and their assemblies, *Appl. Phys. Lett.* **101**, 012409 (2012).



- [14] K. Rohith Vinod, P. Saravanan, M. Sakar, V. T. P. Vinod, M. Cernik, and S. Balakumar, Large scale synthesis and formation mechanism of highly magnetic and stable iron nitride ( $\epsilon$ -Fe<sub>3</sub>N) nanoparticles, *RSC Adv.* **5**, 56045 (2015).
- [15] A. A. El-Gendy, M. Bertino, D. Clifford, M. Qian, S. N. Khanna, and E. E. Carpenter, Experimental evidence for the formation of CoFe<sub>2</sub>C phase with colossal magnetocrystalline-anisotropy, *Appl. Phys. Lett.* **106**, 213109 (2015).
- [16] S. Pal, K. Skokov, T. Groeb, S. Ener, and O. Gutfleisch, Properties of magnetically semi-hard (Fe<sub>x</sub>Co<sub>1-x</sub>)<sub>3</sub>B compounds, *J. Alloys Compd.* **696**, 543 (2017).
- [17] S. Wu, B. Balamurugan, X. Zhao, S. Yu, M. C. Nguyen, Y. Sun, S. Valloppilly, D. J. Sellmyer, K. Ho, and C. Wang, Exploring new phases of Fe<sub>3-x</sub>Co<sub>x</sub>C for rare-earth-free magnets, *J. Phys. D Appl. Phys.* **50**, 215005 (2017).
- [18] J. Mohapatra, M. Xing, J. Elkins, and J. P. Liu, Hard and semi-hard magnetic materials based on cobalt and cobalt alloys, *J. Alloys Compd.* **824**, 153874 (2020).
- [19] P. V. Marshall, Z. Alptekin, S. D. Thiel, D. Smith, Y. Meng, and J. P. S. Walsh, High-Pressure Synthesis of Bulk Cobalt Cementite, Co<sub>3</sub>C, *Chem. Mater.* **33**, 9601 (2021).
- [20] H.-j. Choe, T. Terai, T. Fukuda, T. Kakeshita, S. Yamamoto, and M. Yonemura, Easy axis of magnetization of Fe<sub>3</sub>C prepared by an electrolytic extraction method, *J. Magn. Magn. Mater.* **417**, 1 (2016).
- [21] M. E. Nicholson, Solubility of boron in Fe<sub>3</sub>C and variation of saturation magnetization, curie temperature, and lattice parameter of Fe<sub>3</sub>(C,B) with composition, *JOM* **9**, 1 (1957).
- [22] A. Tsuzuki, S. Sago, S. I. Hirano, and S. Naka, High temperature and pressure preparation and properties of iron carbides Fe<sub>7</sub>C<sub>3</sub> and Fe<sub>3</sub>C, *J. Mater. Sci.* **19**, 2513 (1984).
- [23] H. Bhadeshia, Cementite, *Int. Mater. Rev.* **65**, 1 (2020).
- [24] K. N. Mikhalev, A. Yu. Germov, E. Yu. Medvedev, A. P. Gerashchenko, A. E. Ermakov, M. A. Uimin, S. I. Novikov, T. V. D'yachkova, A. P. Tyutyunnik, and Yu. G. Zainulin, Magnetic State and Phase Composition of Co<sub>3</sub>C Nanoparticles, *Phys. Met. Metallogr.* **120**, 930 (2019).
- [25] V. G. Harris, Y. Chen, A. Yang, S. Yoon, Z. Chen, A. L. Geiler, J. Gao, C. N. Chinnasamy, L. H. Lewis, C. Vittoria, E. E. Carpenter, K. J. Carroll, R. Goswami, M. A. Willard, L. Kurihara, M. Gjoka, and O. Kalogirou, High coercivity cobalt carbide nanoparticles processed via polyol reaction: A new permanent magnet material, *J. Phys. Appl. Phys.* **43**, 165003 (2010).
- [26] Z. Turgut, M. S. Lucas, S. Leontsev, S. L. Semiatin, and J. Horwath, Metastable Co<sub>3</sub>C nanocrystalline powder produced via reactive ball milling: Synthesis and magnetic properties, *J. Alloys Compd.* **676**, 187 (2016).
- [27] A. A. El-Gendy, M. Qian, Z. J. Huba, S. N. Khanna, and E. E. Carpenter, Enhanced magnetic anisotropy in cobalt-carbide nanoparticles, *Appl. Phys. Lett.* **104**, 023111 (2014).
- [28] A. A. El-Gendy, T. Almuqaiteeb, and E. E. Carpenter, Co<sub>x</sub>C nanorod magnets: highly magnetocrystalline anisotropy with lower curie temperature for potential applications, *J. Magn. Magn. Mater.* **348**, 136 (2013).
- [29] A. Kagawa and T. Okamoto, Lattice Parameters of Cementite in Fe-C-X (X = Cr, Mn, Mo, and Ni) Alloys, *Trans. Jpn. Inst. Met.* **20**, 659 (1979).
- [30] P. Schaaf, S. Wiesen, and U. Gonser, Mössbauer study of iron carbides: Cementite (Fe, M)<sub>3</sub>C (M = Cr, Mn) with various manganese and chromium contents, *Acta Metall. Mater.* **40**, 373 (1992).
- [31] M. Umemoto, Z. G. Liu, K. Masuyama, and K. Tsuchiya, Influence of alloy additions on production and properties of bulk cementite, *Scripta Materialia* **45**, 391 (2001).
- [32] X. Wang, P. Zhang, W. Wang, X. Lei, and H. Yang, Fe<sub>3</sub>C and Mn doped Fe<sub>3</sub>C nanoparticles: Synthesis, morphology and magnetic properties, *RSC Adv.* **5**, 57828 (2015).
- [33] S. A. Rounaghi, D. E. P. Vanpoucke, E. Esmaeili, S. Scudino, and J. Eckert, Synthesis, characterization and thermodynamic stability of nanostructured  $\epsilon$ -iron carbonitride powder prepared by a solid-state mechanochemical route, *J. Alloys Compd.* **778**, 327 (2019).
- [34] W. Zhang, Z. Lv, Z. Shi, S. Sun, Z. Wang, and W. Fu, Electronic, magnetic and elastic properties of  $\epsilon$ -phases Fe<sub>3</sub>X (X = B, C, N) from density-functional theory calculations, *J. Magn. Magn. Mater.* **324**, 2271 (2012).
- [35] L. Hui, Z.-Q. Chen, Z. Xie, and C. Li, Stability, Magnetism and Hardness of Iron Carbides from First-Principles Calculations, *J. Supercond. Nov. Magn.* **31**, 353 (2018).
- [36] N. I. Medvedeva, I. R. Shein, M. A. Konyaeva, and A. L. Ivanovskii, Effect of chromium on the electronic structure and magnetic properties of cementite, *Phys. Metals Metallogr.* **105**, 568 (2008).
- [37] I. R. Shein, N. I. Medvedeva, and A. L. Ivanovskii, Electronic structure and magnetic properties of Fe<sub>3</sub>C with 3d and 4d impurities, *Phys. Status Solidi B* **244**, 1971 (2007).
- [38] O. Buggenhoudt, T. Schuler, C.-C. Fu, and J.-L. Béchade, Predicting carbon diffusion in cementite from first principles, *Phys. Rev. Mater.* **5**, 063401 (2021).
- [39] C. M. Fang, M. A. van Huis, and H. W. Zandbergen, Structural, electronic, and magnetic properties of iron carbide Fe<sub>7</sub>C<sub>3</sub> phases from first-principles theory, *Phys. Rev. B* **80**, 224108 (2009).
- [40] A. Dick, F. Körmann, T. Hickel, and J. Neugebauer, Ab initio based determination of thermodynamic properties of cementite including vibronic, magnetic, and electronic excitations, *Phys. Rev. B* **84**, 125101 (2011).
- [41] I. R. Shein, N. I. Medvedeva, and A. L. Ivanovskii, Electronic and structural properties of cementite-type M<sub>3</sub>X (M=Fe, Co, Ni; X=C or B) by first principles calculations, *Phys. B Condens. Matter* **371**, 126 (2006).
- [42] W. C. Chiou Jr and E. A. Carter, Structure and stability of Fe<sub>3</sub>C-cementite surfaces from first principles, *Surf. Sci.* **530**, 88 (2003).
- [43] H. Faraoun, Y. Zhang, C. Esling, and H. Aourag, Crystalline, electronic, and magnetic structures of  $\theta$ -Fe<sub>3</sub>C,  $\chi$ -Fe<sub>5</sub>C<sub>2</sub>, and  $\eta$ -Fe<sub>2</sub>C from first principle calculation, *J. Appl. Phys.* **99**, 093508 (2006).
- [44] D. Odkhuu, N. Tsogbadrakh, A. Dulmaa, N. Otgonzul, and D. Naranchimeg, Substitution- and strain-induced magnetic phase transition in iron carbide, *J. Korean Phys. Soc.* **69**, 1335 (2016).
- [45] F. Chen, H. Jiang, Y. Zhang, S. Tian, Y. Yang, R. Zhang, H. Zhong, and X. Tang, First-principles calculation of bonding and hydrogen trapping mechanism of Fe<sub>3</sub>C/ $\alpha$ -Fe interface, *J. Mater. Res. Technol.* **26**, 6782

- (2023).
- [46] X. Wu, Q. Tian, W. Shen, X. Xu, and J. Fu, An Atomistic Structure of Cementite ( $M_3C$ ,  $M=Fe, Cr, Mn$ ) in Carbon Steel, *Phys. Metals Metallogr.* **124**, 1404 (2023).
- [47] X. Yuan, Y. Zhou, C. Huo, W. Guo, Y. Yang, Y. Li, and X. Wen, Crystal structure prediction approach to explore the iron carbide phases: Novel crystal structures and unexpected magnetic properties, *J. Phys. Chem. C* **124**, 17244 (2020).
- [48] Z. Lv, F. Zhang, S. Sun, Z. Wang, P. Jiang, W. Zhang, and W. Fu, First-principles study on the mechanical, electronic and magnetic properties of  $Fe_3C$ , *Comput. Mater. Sci.* **44**, 690 (2008).
- [49] M. A. Konyaeva and N. I. Medvedeva, Electronic structure, magnetic properties, and stability of the binary and ternary carbides  $(Fe,Cr)_3C$  and  $(Fe,Cr)_7C_3$ , *Phys. Solid State* **51**, 2084 (2009).
- [50] Z. Lv, W. Fu, S. Sun, X. Bai, Y. Gao, Z. Wang, and P. Jiang, First-principles study on the electronic structure, magnetic properties and phase stability of alloyed cementite with Cr or Mn, *J. Magn. Magn. Mater.* **323**, 915 (2011).
- [51] J.-p. Yang, J. Chen, W. Li, P.-d. Han, and L.-n. Guo, First-principles study on electronic structure, magnetic and dielectric properties of Cr-doped  $Fe_3C$ , *J. Cent. South Univ.* **23**, 2173 (2016).
- [52] C. Wang, Z. Lv, W. Fu, Y. Li, S. Sun, and B. Wang, Electronic properties, magnetic properties and phase stability of alloyed cementite  $(Fe, M)_3C$  ( $M=Co, Ni$ ) from density-functional theory calculations, *Solid State Sci.* **13**, 1658 (2011).
- [53] Y. Gao, B. Wang, M. Guo, Z. Lv, S. Sun, R. Zhang, and W. Fu, First-principles study on surface structural, magnetic and electronic properties of alloyed cementite with Co or Ni, *Comput. Mater. Sci.* **85**, 154 (2014).
- [54] C. K. Ande and M. H. Sluiter, First-principles calculations on stabilization of iron carbides ( $Fe_3C$ ,  $Fe_5C_2$ , and  $\eta$ - $Fe_2C$ ) in steels by common alloying elements, *Metall. Mater. Trans. A* **43**, 4436 (2012).
- [55] V. Razumovskiy and G. Ghosh, A first-principles study of cementite ( $Fe_3C$ ) and its alloyed counterparts: Structural properties, stability, and electronic structure, *Comput. Mater. Sci.* **110**, 169 (2015).
- [56] Z. Lv, W. Fu, S. Sun, Z. Wang, W. Fan, and M. Qv, Structural, electronic and magnetic properties of cementite-type  $Fe_3X$  ( $X=B, C, N$ ) by first-principles calculations, *Solid State Sci.* **12**, 404 (2010).
- [57] N. Medvedeva, I. Shein, O. Y. Gutina, and A. Ivanovskii, Simulation of the structural, electronic, and magnetic properties of  $Fe_3C_{1-x}B_x$  borocementites, *Phys. Solid State* **49**, 2298 (2007).
- [58] J. Marciniak, M. Werwiński, and J. Rychły-Gruszecka, First-principles study of the magnetic anisotropy of ultrathin B-, C-, and N-doped FeCo films, *J. Magn. Magn. Mater.* **589**, 171563 (2024).
- [59] D. Fruchart, P. Chaudouet, R. Fruchart, A. Rouault, and J. Senateur, Etudes structurales de composés de type cémentite: Effet de l'hydrogène sur  $Fe_3C$  suivi par diffraction neutronique. Spectrométrie Mössbauer sur  $FeCo_2B$  et  $Co_3B$  dopés au  $^{57}Fe$ , *J. Solid State Chem.* **51**, 246 (1984).
- [60] H. L. Yakel, Crystal structures of stable and metastable iron-containing carbides, *Int. Met. Rev.* **30**, 17 (1985).
- [61] K. Koepnik and H. Eschrig, Full-potential nonorthogonal local-orbital minimum-basis band-structure scheme, *Phys. Rev. B* **59**, 1743 (1999).
- [62] I. Opahle, K. Koepnik, and H. Eschrig, Full-potential band-structure calculation of iron pyrite, *Phys. Rev. B* **60**, 14035 (1999).
- [63] J. P. Perdew, K. Burke, and M. Ernzerhof, Generalized Gradient Approximation Made Simple, *Phys. Rev. Lett.* **77**, 3865 (1996).
- [64] K. Momma and F. Izumi, *VESTA*: A three-dimensional visualization system for electronic and structural analysis, *J. Appl. Crystallogr.* **41**, 653 (2008).
- [65] U. Von Barth and L. Hedin, A local exchange-correlation potential for the spin polarized case. i, *J. Phys. C: Solid State Phys.* **5**, 1629 (1972).
- [66] J. P. Perdew and A. Zunger, Self-interaction correction to density-functional approximations for many-electron systems, *Phys. Rev. B* **23**, 5048 (1981).
- [67] J. P. Perdew and Y. Wang, Accurate and simple analytic representation of the electron-gas correlation energy, *Phys. Rev. B* **45**, 13244 (1992).
- [68] J. Snarski-Adamski and M. Werwiński, Searching for magnetically hard monoborides (and finding a few): A first-principles investigation, arXiv preprint [10.48550/arXiv.2403.00138](https://arxiv.org/abs/10.48550/arXiv.2403.00138) (2024).
- [69] O. V. Zhdanova, M. B. Lyakhova, and Yu. G. Pastushenkov, Magnetic properties and domain structure of FeB single crystals, *Met. Sci. Heat Treat.* **55**, 68 (2013).
- [70] B. L. Gyorffy, A. J. Pindor, J. Staunton, G. M. Stocks, and H. Winter, A first-principles theory of ferromagnetic phase transitions in metals, *J. Phys. F Met. Phys.* **15**, 1337 (1985).
- [71] J. Kudrnovský, I. Turek, V. Drchal, F. Máca, P. Weinberger, and P. Bruno, Exchange interactions in III-V and group-IV diluted magnetic semiconductors, *Phys. Rev. B* **69**, 115208 (2004).
- [72] P. Soven, Coherent-potential model of substitutional disordered alloys, *Phys. Rev.* **156**, 809 (1967).
- [73] V. Heine, J. H. Samson, and C. M. M. Nex, Theory of local magnetic moments in transition metals, *J. Phys. F Met. Phys.* **11**, 2645 (1981).
- [74] S. Meschel and O. Kleppa, Standard enthalpies of formation of some 3d transition metal carbides by high temperature reaction calorimetry, *J. Alloys Compd.* **257**, 227 (1997).
- [75] E. Martinez-Teran, A. K. Cordeiro, and A. A. El-Gendy, Nucleation of  $Co_3C$  Magnetic Nanoparticles Using Supercritical Condition of Ethanol, *JOM* **71**, 4940 (2019).
- [76] A.-M. Zieschang, J. D. Bocarsly, J. Schuch, C. V. Reichel, B. Kaiser, W. Jaegermann, R. Seshadri, and B. Albert, Magnetic and Electrocatalytic Properties of Nanoscale Cobalt Boride,  $Co_3B$ , *Inorg. Chem.* **58**, 16609 (2019).
- [77] V. A. Barinov, V. A. Tsurin, V. A. Kazantsev, and V. T. Surikov, Carbonization of  $\alpha$ -Fe upon mechanical alloying, *Phys. Met. Metallogr.* **115**, 53 (2014).
- [78] G. Le Caer, J. M. Dubois, M. Pijolat, V. Perrichon, and P. Bussiere, Characterization by Moessbauer spectroscopy of iron carbides formed by Fischer-Tropsch synthesis, *J. Phys. Chem.* **86**, 4799 (1982).
- [79] I. Turek, J. Kudrnovský, G. Bihlmayer, and S. Blügel, Ab initio theory of exchange interactions and the Curie temperature of bulk Gd, *J. Phys.: Condens. Matter* **15**, 2771 (2003).
- [80] H. Ebert, D. Ködderitzsch, and J. Minár, Calculating condensed matter properties using the KKR-Green's function method—recent developments and applica-

- tions, *Rep. Prog. Phys.* **74**, 096501 (2011).
- [81] L. Ke, K. D. Belashchenko, M. van Schilfhaarde, T. Kotani, and V. P. Antropov, Effects of alloying and strain on the magnetic properties of  $\text{Fe}_{16}\text{N}_2$ , *Phys. Rev. B* **88**, 024404 (2013).
- [82] R. Wu and A. J. Freeman, Spin-orbit induced magnetic phenomena in bulk metals and their surfaces and interfaces, *J. Magn. Magn. Mater.* **200**, 498 (1999).
- [83] D. Jiang and E. A. Carter, Carbon dissolution and diffusion in ferrite and austenite from first principles, *Phys. Rev. B* **67**, 214103 (2003).
- [84] S. N. Budko and M. V. Mamonova, Calculation of the exchange integrals for  $\text{Co}_{1-x}\text{Ni}_x$  alloy by Korring-Kohn-Rostoker method, *J. Phys.: Conf. Ser.* **1389**, 012144 (2019).
- [85] J. Snarski-Adamski and M. Werwiński, Effect of transition metal doping on magnetic hardness of  $\text{CeFe}_{12}$ -based compounds, *J. Magn. Magn. Mater.* **554**, 169309 (2022).
- [86] T. Burkert, L. Nordström, O. Eriksson, and O. Heinonen, Giant magnetic anisotropy in tetragonal  $\text{FeCo}$  alloys, *Phys. Rev. Lett.* **93**, 027203 (2004).
- [87] A. Edström, M. Werwiński, D. Iuşan, J. Ruzs, O. Eriksson, K. Skokov, I. Radulov, S. Ener, M. Kuz'Min, J. Hong, *et al.*, Magnetic properties of  $(\text{Fe}_{1-x}\text{Co}_x)_2\text{B}$  alloys and the effect of doping by 5d elements, *Phys. Rev. B* **92**, 174413 (2015).
- [88] W. Marciniak and M. Werwiński, Structural and magnetic properties of  $\text{Fe-Co-C}$  alloys with tetragonal deformation: A first-principle study, *Phys. Rev. B* **108**, 214433 (2023).
- [89] M. C. Cadeville and E. Daniel, Sur la structure électronique de quelques borures d'éléments de transition, *J. Phys.* **27**, 449 (1966).
- [90] C. T. Chen, Y. U. Idzerda, H.-J. Lin, N. V. Smith, G. Meigs, E. Chaban, G. H. Ho, E. Pellegrin, and F. Sette, Experimental Confirmation of the X-Ray Magnetic Circular Dichroism Sum Rules for Iron and Cobalt, *Phys. Rev. Lett.* **75**, 152 (1995).
- [91] M. Däne, S. K. Kim, M. P. Surh, D. Åberg, and L. X. Benedict, Density functional theory calculations of magnetocrystalline anisotropy energies for  $(\text{Fe}_{1-x}\text{Co}_x)_2\text{B}$ , *J. Phys.: Condens. Matter* **27**, 266002 (2015).
- [92] T. Sourmail, Near equiatomic  $\text{FeCo}$  alloys: Constitution, mechanical and magnetic properties, *Prog. Mater. Sci.* **50**, 816 (2005).
- [93] M. Ležaić, Ph. Mavropoulos, and S. Blügel, First-principles prediction of high Curie temperature for ferromagnetic  $\text{bcc-Co}$  and  $\text{bcc-FeCo}$  alloys and its relevance to tunneling magnetoresistance, *Appl. Phys. Lett.* **90**, 082504 (2007).
- [94] H. Akai, Nuclear spin-lattice relaxation of impurities in ferromagnetic iron, *Hyperfine Interact.* **43**, 253 (1988).
- [95] P. H. Dederichs, R. Zeller, H. Akai, and H. Ebert, Ab-initio calculations of the electronic structure of impurities and alloys of ferromagnetic transition metals, *J. Magn. Magn. Mater.* **100**, 241 (1991).
- [96] J. Snarski-Adamski, J. Rychły, and M. Werwiński, Magnetic properties of 3d, 4d, and 5d transition-metal atomic monolayers in  $\text{Fe/TM/Fe}$  sandwiches: Systematic first-principles study, *J. Magn. Magn. Mater.* **546**, 168828 (2022).
- [97] H. Du, A reevaluation of the  $\text{Fe-N}$  and  $\text{Fe-C-N}$  systems, *J. Phase Equilibria* **14**, 682 (1993).
- [98] D. Hedlund, J. Cedervall, A. Edström, M. Werwiński, S. Kontos, O. Eriksson, J. Ruzs, P. Svedlindh, M. Sahlberg, and K. Gunnarsson, Magnetic properties of the  $\text{Fe}_5\text{SiB}_2 - \text{Fe}_5\text{PB}_2$  system, *Phys. Rev. B* **96**, 094433 (2017).
- [99] M. B. Lourenço, M. D. Carvalho, P. Fonseca, T. Gasche, G. Evans, M. Godinho, and M. M. Cruz, Stability and magnetic properties of cobalt nitrides, *J. Alloys Compd.* **612**, 176 (2014).
- [100] L. Wu, D. Shi, S. Yan, W. Qiao, W. Zhong, and Y. Du, Iron-doped cobalt nitride nanoparticles ( $\text{Fe-Co}_3\text{N}$ ): An efficient electrocatalyst for water oxidation, *Int. J. Hydrog. Energy* **46**, 2086 (2021).
- [101] H. A. Wriedt, N. A. Gokcen, and R. H. Nafziger, The  $\text{Fe-N}$  (Iron-Nitrogen) system, *Bull. Alloy Phase Diagr.* **8**, 355 (1987).